UNIVERSITÀ DEGLI STUDI DI PADOVA

Dip. TERRITORIO E SISTEMI AGRO-FORESTALI

Corso di laurea in Scienze Forestali e Ambientali

ANALISI MULTITEMPORALE (2006-2016) DI UNA FRANA DEL BACINO DEL RIO CORDON

MULTI-TEMPORAL (2006-2016) ANALYSIS OF A LANDSLIDE OF THE RIO CORDON CATCHMENT

Relatore:
Prof. Paolo Tarolli
Correlatore:
Dott. Marco Cavalli

Laureanda
Jessica De Marco

Matricola n.
1106349

ANNO ACCADEMICO 2015/2016

RIASSUNTO

Nel presente elaborato è stata effettuata un'analisi multitemporale, mediante l'impiego di sensori remoti, di una frana localizzata nel bacino del Rio Cordon per il periodo 2006-2016. Il bacino del Rio Cordon è sito nel Comune di Selva di Cadore (Belluno, BL) a monte della confluenza col Torrente Fiorentina. L'area analizzata è situata in sinistra idrografica nei pressi del sentiero CAI 466 fra i 1800 e i 2010 metri di quota.

L'evento che ha dato origine alla frana soggetta a studio è avvenuto nel 2001. A causa dello scioglimento nivale, si è verificato uno smottamento che ha dato in seguito origine ad un mud flow, il quale si è poi depositato nella zona adiacente al corso d'acqua del Rio Cordon. Nella presente tesi verrà analizzata esclusivamente l'area interessata dalla frana e non quella interessata da mud flow, in quanto si dispone di dati multitemporali riguardanti solamente la prima area.

La tesi analizza il movimento di sedimento e l'individuazione di zone di erosione/accumulo ed è articolata in quattro fasi.

Nella prima fase della ricerca sono stati recuperati, per l'area di studio, dati ad alta risoluzione, ricavati con tecnologie LiDAR (sia ALS che TLS) risalenti agli ultimi anni. Sono stati recuperati dati prodotti negli anni 2006, 2010 e 2011.

Si è poi proceduto con la seconda fase, ossia l'analisi della situazione attuale dell'area di studio e la produzione di un database ad alta risoluzione. Per effettuare i rilievi si è utilizzata la tecnica Structure from Motion ed è stata prodotta una nuvola di punti georeferenziata dell'area.

I vari dati sono poi stati co-registrati nella terza fase utilizzando il software CloudCompare al fine di ottenere, per ogni coppia di nuvole di punti, la migliore sovrapposizione.

Nell'ultima fase, le nuvole di punti sono state trasformate in DTM ed è stata effettuata l'analisi DEM of Difference (DoD) alle coppie di DTM (Digital Terrain Model) utilizzando Geomorphic Change Detection (GCD), un plug-in di ArcGIS. Questo tool si basa sulla formula di Wheaton (2010) e consente l'inserimento di una soglia limite sotto la quale la differenza di quota fra i due DTM non è considerata.

I due passaggi finali sono strettamente legati e, assieme, costituiscono un processo "try and error", che viene applicato finché non si è ottenuto un risultato soddisfacente. I risultati sono stati costantemente confrontati con le foto storiche reperite, al fine di constatarne la plausibilità e veridicità.

Nel complesso l'applicazione di tale procedura è risultata positiva e sono stato ottenuti risultati interessanti. Un DoD in particolare (2006-2011) ha mostrato la rappresentazione verosimile

dell’evoluzione della frana, delineando le zone di erosione e di accumulo effettivamente riscontrate nell’analisi fotografica storica effettuata. Sulla base dei dati acquisiti si prospettano analisi future dell’area al fine di utilizzare diverse tecnologie e monitorare l’evoluzione futura dell’area con i dovuti accorgimenti.

ABSTRACT

In this paper was made a multi-temporal analysis of a landslide using remote sensing sensors. The landslide is placed in the Rio Cordon catchment for the period 2006-2016. The Cordon catchment is located in Selva di Cadore municipality (Belluno, BL) above the confluence with Fiorentina creek. The study area is located in the left hand side close to the hiking path CAI 466, with an elevation ranging between 2010 and 1800 meters above the level of the see.

The event that had originated the landslide happened in 2001. The snow melted and caused a landslide that activated a mud flow along the downhill area. The mud flow stopped close to the Cordon steam area. In this thesis only the landslide area will be analyzed; the mud flow area will be not analyzed because, only for the first one mentioned, there are available multi-temporal data.

This work examines sediments movements and identifies both erosional and depositional areas. This thesis is divided into four phases.

In the first phase, high-resolution data of the last years were collected for the study area.

Datasets from 2006, 2010, and 2011 were found and these data were made by LiDAR technique (ALS and TLS).

The second phase consisted in analyzing the current condition of the study area and in producing a high-resolution database. The new database was created by using the Structure from Motion (SfM) photogrammetric technique. Using SfM technique, a geo-referred high density point cloud was produced.

Each dataset was co-registered in the third phase to obtain the best overlapping for each pair of clouds. This process was made by using CloudCompare software.

During the fourth phase, the co-registered point clouds were converted into DTM (Digital Terrain Model) and a DEM of Difference analysis (DoD) was done using Geomorphic Change Detection (GCD) which is a ArcGIS plugin based on Wheaton's formula (2010). This technique allows to insert a threshold under which the DTM differences are not considered.

The third and the fourth phase are strictly connected because they constitute a "try and error" process which is applied as long as a satisfying result is obtained. The results were also compared with historical photographs to check the consistency of the results.

Overall, the application of this procedure was positive and the result obtained was interesting.

One DoD in particular (2006-2011) showed a plausible representation of the study area evolution highlighting erosional and depositional areas which are also identified in the analysis of historical pictures.

To sum up, future analyses of the study area are supposed to use different technologies and to monitor the future study area evolution with the proper devices basing on the data acquired.

The author wishes to thank Giulia Costan Davara for reviewing the English text.

TABLE OF CONTENTS

LIST OF FIGURES

LIST OF TABLES

1. INTRODUCTION

Landslides are one of the most dangerous phenomena in the world, often causing fatalities and economic damages. There is not only one definition of this phenomenon, it changes based on the discipline that is studying a landslide and its point of view.

D.M. Cruden (1991) has done an interesting research about the origins of the landslide word and its definition. He found that landslide is an american word and in English language the term used to define this kind of process was "landslips". As reported by Cruden (1991) for the Working Party on World Landslide Inventory, the informal definition of landslide implies "the movement of a mass of rocks, earth or debris down a slope".

Actually "the Landslides Handbook- a Guide to Understanding Landslide" (2008), produced by U.S. Department of the Interior and the U.S. Geological Survey (USGS), defines landslide as "a general term used to describe the downslope movement of soil, rock, and organic materials under the effects of gravity and also the landform" formed from this kind of movement. This phenomenon exists due to gravity so also underwater, because not everyone knows that "some of the world's largest landslides have occurred on the steep, submerged volcanic slopes of the Hawaiian Islands" (Lee, 1989)

In Figure 1.1 it is possible to observe all the typical parts of a landslide and their terminology.

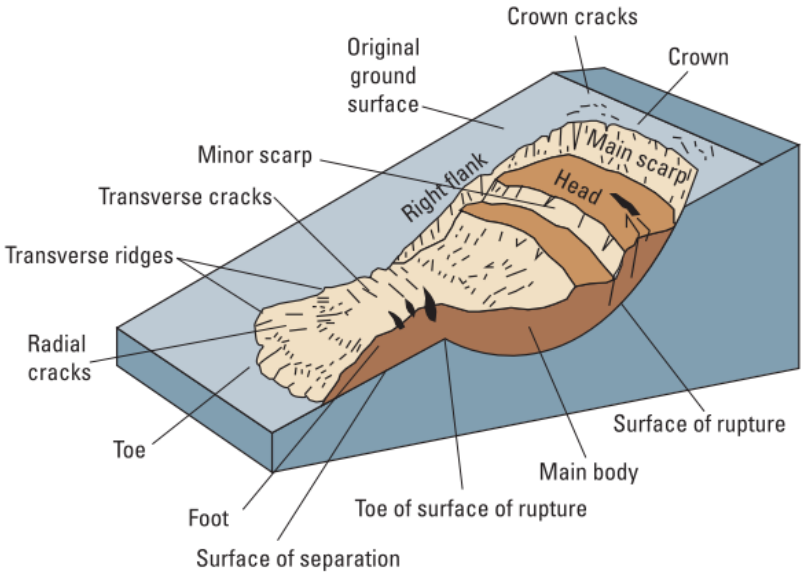

Figure 1.1This is an illustration of a rotational landslide which has evolved into an earthflow. It illustrates commonly used labels for the parts of a landslide (from Varnes, 1978, Reference 43) with the technical terminology used by USGS

According to Varnes' landslide classification (1978), the two parameters to identify a landslide are the following: the type of material (rock, earth, soil, mud, and debris) and the type of movement of the landslide (fall, topple, slide, spread, or flow). However, it usually happens that a landslide embraces different types of movements and materials, so understanding characteristics of each basic category of landslide is a fundamental step to prevent risks and to have an appropriate knowledge about this topic.
Below are listed the definitions of each type of material that characterize a landslide:

- Rock: it is "a hard or firm mass that was intact and in its natural place before the initiation of movement";
- Soil: it is "an aggregate of solid particles, generally of minerals and rocks, that either was transported or was formed by the weathering of rock in place. Gases or liquids filling the pores of the soil form part of the soil";
- Earth: it "describes material in which 80% or more of the particles are smaller than 2mm, the upper limit of sand sized particles";
- Mud: it "describes material in which 80% or more of the particles are smaller than 0.06mm, the upper limit of silt sized particles";
- Debris: it "contains a significant proportion of coarse material; 20% to 80% of the particles are larger than 2mm, and the remainder are less than 2mm".

(Varnes, 1978)

Further details on classification scheme can be found in Varnes (1978) and in "Landslides Handbook-a Guide to Understanding Landslide"(Highland and Bobrowsky 2008).
The type of movement describes the actual internal mechanics of how the landslide mass is displaced and, as already said, there are five kind of kinematic movements (Figure 1.2):

- Falls: with this term is defined a movement caused by gravity placed on a cliff or a steep slope where a mass of any size is detached. These rocks move usually through the air doing a free fall, leaping, bounding, and rolling according with the surface;
- Topples: this movement is different from falls and "consists of the forward rotation of a unit or units about some pivot point, below or low in the unit, under the action of gravity and forces exerted by adjacent units or by fluids in cracks. It is tilting without collapse." (Varnes, 1978)
- Spreads: the "dominant mode of movement is lateral ex- tension accommodated by shear or tensile fractures" (Varnes, 1978);

- Slides: this movement is caused by a shear strain along one or more layers of terrain and this force is more intense than the cohesion between the layer where this force is applied and another layer which is below. This type of landslide is subdivided into rotational slides and transitional slides based on the morphology of the sliding surface;
- Flows: unconsolidated material can keep the form of a flow, the movement can be fast or slow, wet or dry, and in many cases the behavior of the movement seems to be the same as viscous fluids.

These definitions were resume by Varnes (1978).

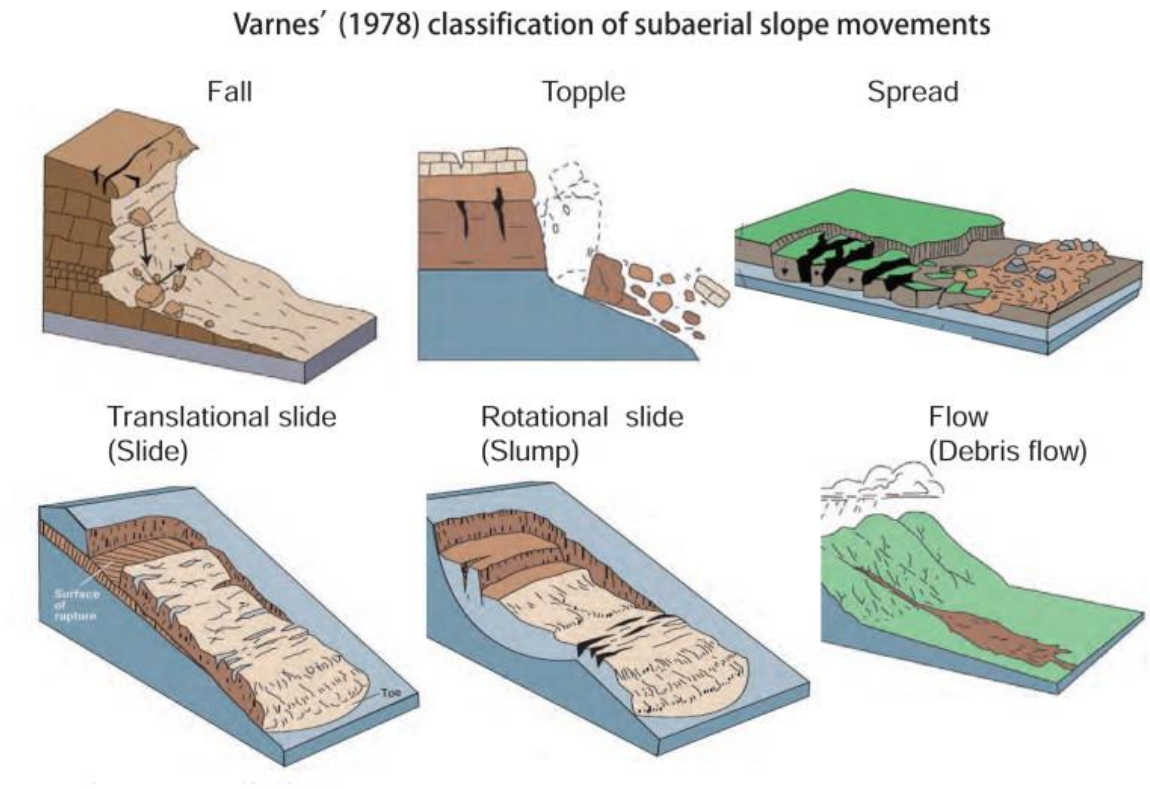

Figure 1.2 different kind of landslide by Varnes' classification (198) (source: https://www.researchgate.net)

Landslides are really important sources of sediments in a catchment.

Not only sediment source areas cover a small portion of mountainous surface (e.g. Cavalli et al, 2016), but also have an essential role in transport sediment. Just thinking about the steps necessary to assessing sediment delivery in a catchment: identification sediment source type, extent, and location of sediment sources degree of linkage between sources and channel network are key steps (Cavalli et al, 2016). These kind of area show high frequency of erosion and instability; in addiction, they produce the main amount of sediment in mountainous basins.

Erosion phenomenon in sediment source usually involves at least one of these mechanical triggers:

- Temperature leap which happens especially in high altitude where daily changes between light and shadows or between day and night can freeze or melt water inside interstice of rocks and cause crack of material;
- Glacier movements occur because of a rubbing between the glacier and terrain; as a result, there is an erosion and transport of soil;
- Wind causes erosion due to ablation in desert areas;
- Rainfall is the main cause of soil erosion in alpine areas and the main trigger for landslide.

Understanding sediment source dynamics on hillslope and along colluvial channels is a relevant information to estimate sediment supply to main rivers. Knowing the possible behavior of each type of sediment sources, it is possible to have a better understanding of a potential amount of moved sediment in a basin and identify critical areas that need to be safeguard. It is also possible to use these data to scale down hydrological infrastructure and to undertake sediment management strategies in order to avoid high risk for human life. The lack of information on sediment dynamics and on transport in the mountainous areas can have serious consequences in downstream areas. The management of mountainous areas is essential to prevent disasters and to protect people.
Sediment source behavior is very challenging, there are a lot of questions with blurry answers; some examples are the following: how will these areas react in different kind of situation and with different kind of runoff? How they change over time?

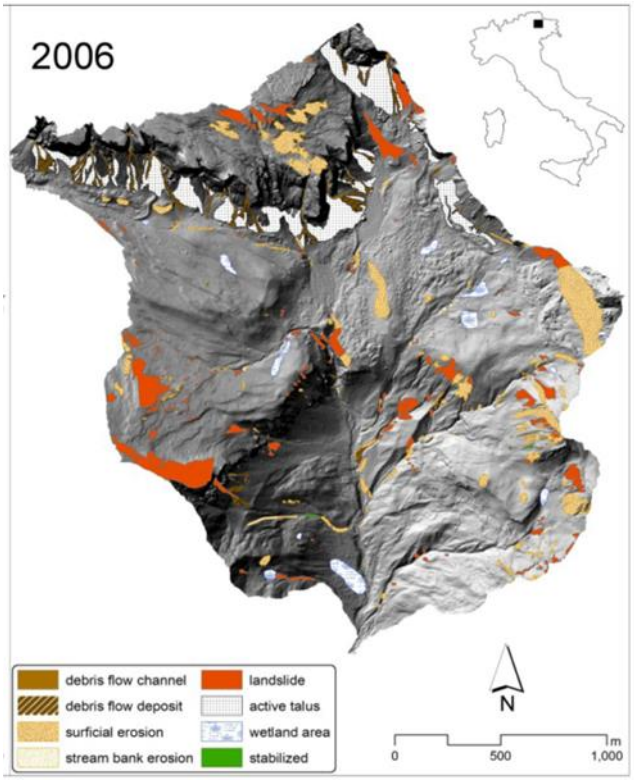

Figure 1.3 an example of sediment source inventory (Cavalli et all. 2006)

The most used way to approach landslide phenomena and to understand how they work is following the process over time; for example, monitoring continuously phenomena during the whole year. The time interval of monitoring depends on the situation and on the risk generated by the landslide. It can be longer or shorter as a result of a different combination of many factors: celerity of movements of the phenomenon, meteorological conditions, and budget.

Landslides inventories are fundamental resources to provide data to be compared to assess sediment sources changes through time at catchment scale (e.g. Cavalli et al, 2016). They are important to identify high landslide density areas and areas with changing of number or extension or type of landslide. It is really rare starting to study and to monitor an area before the triggering of a landslide or an erosion is visible. When a database is active for an area, it becomes essential to understand in which range of time a precise event started in a specific area and to have an appropriate basilar knowledge about how this phenomenon works through time. Only monitoring the evolution of a phenomenon and crossing how it develops this other characteristics (e.g. meteorological events, geology, slope, vegetation cover…) it is possible to track how it works. Analyzing a large amount of similar cases, it is also possible to extend scale crossing a large amount of cases with similar characteristics to find a connection for erosion behavior.

Using appropriately database is also possible to reduce the risk of this natural hazard: a better knowledge of a landslides location and evolution makes possible to help technicians in risk planning and in infrastructure management of a basin. Having this kind of information is fundamental to understand which infrastructure is needed, in which place, and to scale down it. Make a mistake to choose one of this parameters can make the infrastructure useless; so, this can make the difference between preserve and not preserve human infrastructures and lives.

Landslides inventories need to be based on consolidated approaches and techniques rewired in Guzzetti et al (2012). Using these databases is possible to observe and to study the evolution of the event during a period of time. So, database is one of the key parameters to understand the event and the morphological evolution of the surface displacement field.

If database is so important for understanding landslide phenomenon, the applied methodology to this process is fundamental too. Improving methods, the database is also improving, the quality and intrinsic characteristics of data are changing. So, this means that data are not reached in the same way and not perfectly comparable, this is an important characteristic to take in mind when data are compared and results were taken. Knowing the applied methodology, its characteristics and lacks are necessary to make data comparable and usable. Conventional methods for landslide mapping were mainly based on visual interpretation of stereoscopic aerial photography, aided by field surveys; this type of approach was expensive and it requires time to be applied (Guzzetti et al, 2012). Nowadays

there are a lot of developments in this field and new techniques are coming out, they are based on satellite, airborne, and terrestrial remote sensing techniques.

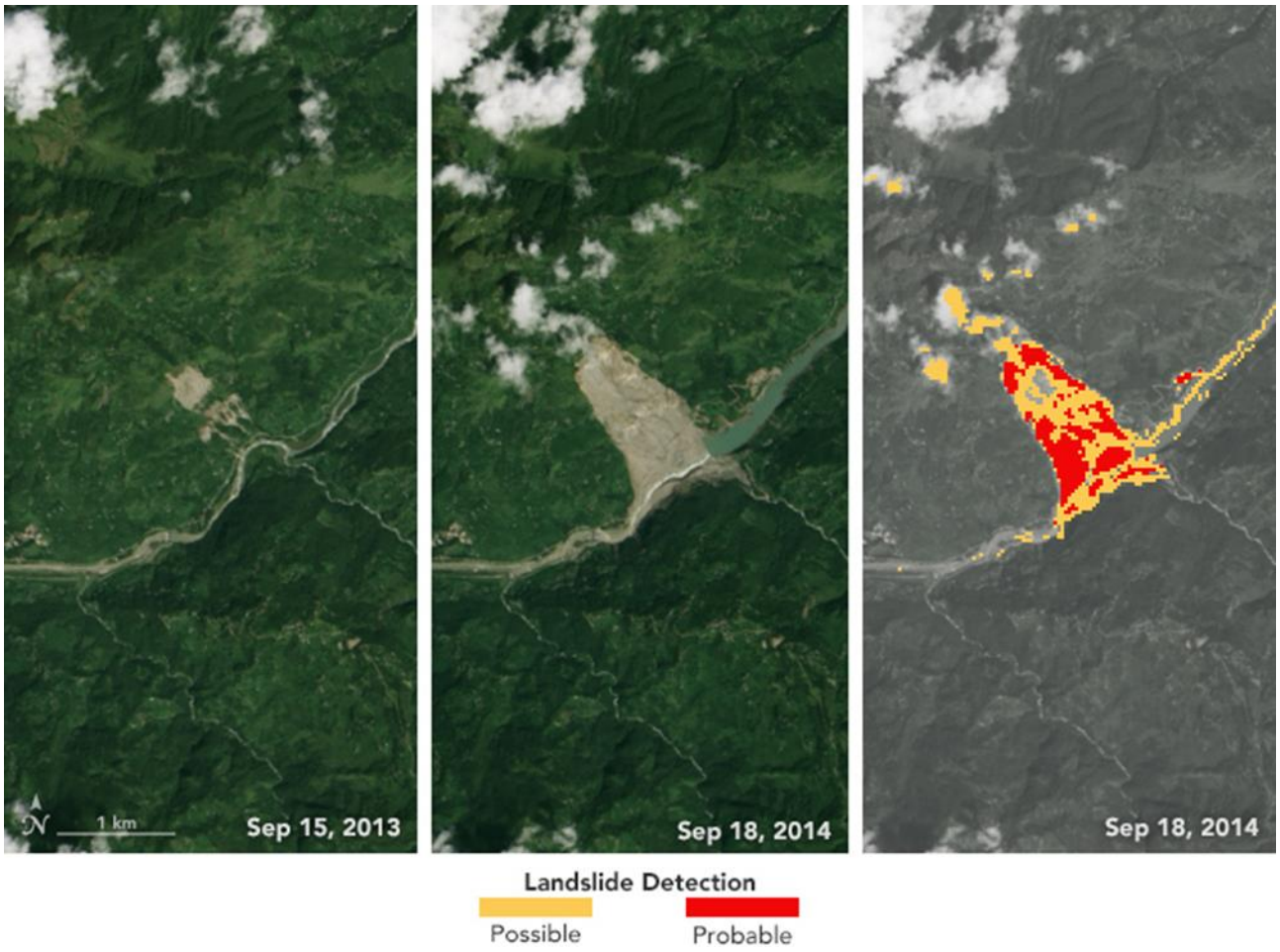

Figure 1.4 example of landslide detection by NASA by analyzing satellite imagery for changes in surface fetures (www.gislounge.com)

There are a lot of monitoring methods which can be used in sediment source monitoring and they can broadly subdivide into two main groups: geodetic and remote-sensing techniques.

Geodetic surveying consists of detecting geometrical changes in the landslide topography by measuring geometric parameters like angles, distances or differences in elevation (Travelletti et al, 2012). This methodology needs to install targets inside and outside of landslide area and measures the position of each target at different times. A positive aspect is that these techniques can be very accurate with a high potential of automation (Foppe et al, 2006; Jaboyedoff et al, 2004; Malet et al, 2002).

Another geodetic technique is dGPS (differential Global Positioning System) which allows to obtain really accurate data during any day-time and with all-weather conditions. In scientific literature there are copious papers that show the efficiency of non-permanent and permanent stations made to monitoring landslides (Brunner et al,2007; Malet et al, 2002; Squarzoni et al, 2005).

The disadvantages of geodetic techniques are the high costs of installation and maintenance of survey network; as a result, these approaches provide only discrete data measurements and the only justification to use them is a real risk for human life.
Surface displacements can be also calculated using remote-sensing methods. Remote sensing was defined a lot of times in research history (Table 1.1).

Table 1.1: some historical definitions of "remote sensing"

Remote sensing has been variously defined but basically it is the art of science of telling something about an object without touching it.(Fischer et al, 1976)
Remote sensing is the acquisition of physical data of an object without touching or contact. (Lintz and Simonett, 1976)
Imagery is acquired with a sensor other than (or in addition to) a conventional camera through which a scheme is recorded, such as by electronic scanning, using radiations outside the normal visual range of the film and camera-microwave, radar, thermal, infrared, ultraviolet, as well as multispectral, special techniques are applied to process and interpret remote sensing imagery for the purpose of producing conventional maps, thematic maps, resources surveys, etc., in the fields of agriculture, archeology, forestry, geography, geology, and other. (American Society of Photogrammetry)
Remote sensing is the observation of a target by a device separated from it by some distance. (Barrett and Curtis, 1976)

Some example of remote sensing techniques applied to this field are interferometry for radar data and image correlation for optical data applied to surface displacement filed of a landslide (Delacourt et al, 2007). These methods developed very fast in the last sixty years and they are still developing, giving great opportunities and possibilities to landslide and sediment source research department. Recently they were applied to different sensors like Lidar, terrestrial laser scanner (TLS) and cameras. These technologies are the most applied in landslide research.
Airborne (ALS) and groundbased (TLS) LiDAR sensors are interesting and promising technologies with rapid development- Laser scanning techniques emerged in 90's and fifteen years ago "datasets from airborne and groundbased laserscanners or LiDAR were released from remote sensing specialists' computer to be used by geoscientists experienced in slope processes and landslide investigations" (Derron and Jaboyedoff, 2010)
LiDAR is also applied in landslide field, giving high opportunities to study this phenomenon with high-resolution and high spatial data to create accurate and precise high-resolution digital elevation

models. The density level mainly depends on the position of sensors in comparison with the studied object.

There are a lot of interesting studies about landslide analysis using TLS (e.g. Lichti and Jamtsho, 2006; Teza et al, 2007).

Figure 1.5 Rendered LiDAR image illustrating deep seated landslide underneath vegetative cover. South Fork Eel River confluence with Tenmile Creek. Image: Collin Bode, 2010. LiDAR: 2004, NCALM. (http://criticalzone.org)

TLS, for example was applied to a multi-temporal study of the Séchilienne Landslide (Kasperski et al, 2010) obtaining an accuracy of 250 mm showing itself as a useful instrument to detect also micro-movements trough time. The most important limitation was that this method only gives information about altitude changes. This was compensated by the object recognition based on 2D transects in the main direction of displacements, completing information and enabling quantification of displacements with an accuracy of +/−30 mm in all directions (Kaspersky et al, 2010).

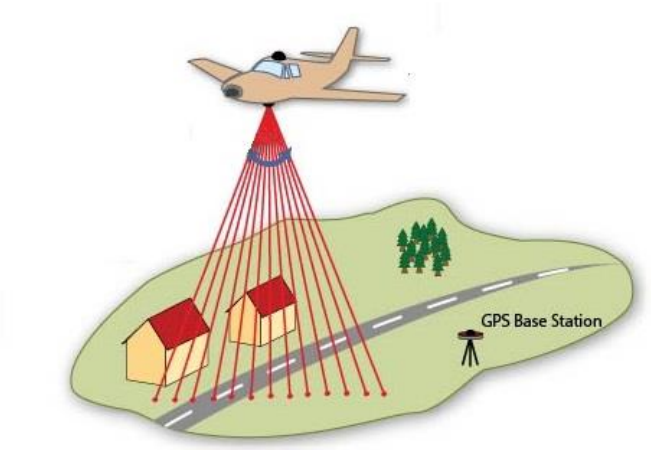

Figure 1.6 a representation of ALS survey

TLS can also be used in not optimal weather condition like rainy days (Travelletti et al, 2008), also in this case TLS shows itself as a really good technology to detect slope movements over a whole

landslide area, but it needs some precaution in field to maximize accuracy: the scans needs to be calibrate on stable areas.

Also ALS received a lot of consideration in the last decade, one of the first application of ALD and DEM to map and model landslide susceptibility was published in 2001 (Dietrich et al, 2001) since this moment, the application of ALS technique increased. In literature is possible to find a lot of studies about ALS technologies applied to landslide (e.g. Razak et al, 2011, 2013; Wang et al, 2013).

Another important methodology used for geoscience analysis is SfM (Structure from Motion) which is an accurate cost-effective method: "85.6% of the SfM data are accurate to within ± 0.5 m of the TLS data." (Westoby et al, 2012). It is used to costal cliff monitoring (James and Robson, 2012), glacial and periglacial processes research (Kääb et al, 2013; Whitehead et al, 2013), volcanic dome and lava flow (Bretar et al, 2013; James and Varley, 2012), gully erosion surveys (Gómez-Gutiérrez et al, 2014), soil micro-topography (Ouédraogo et al, 2014), river analysis (Javernick et al, 2014) and to monitor landslide displacements (e.g. Niethammer et al, 2011; Stumpf et al, 2014; Westoby et al, 2012). Another important characteristic is that it can also be associated with UAV technology (Lucieer et al, 2014; Turneret al, 2015).

There are a lot of remote sensing techniques and instruments to collect morphological data of a sediment source, this will be cleared in Chapter 3.

A clarification is necessary: in this thesis it will be used the International Glossary of Hydrology (WMO and UNESCO, 1998) about the meaning of the "left-hand side " and "right-hand side" for river banks that is "Margin of a channel at the left-hand (right- hand) side when facing downstream". This terminology will be used to identify parts of study area.

In other paragraphs, it will be possible to read "right-hand side of the picture/figure" which is not related with hydrologic terms.

The purpose of this thesis is the analysis of the geomorphic changes occurred in the last ten years in a small landslide placed in the Rio Cordon catchment (North Eastern Italy) using high-resolution Digital Terrain Models (DTMs) derived from different topographic survey techniques like TLS, ALS, and SfM. Trying to quantify potential movements and changes in the amount of sediments in this landslide through time comparing DEM produced with these techniques between 2006 and 2016.

2. STUDY AREA

The study area of this thesis is a small landslide placed in a headwater catchment of Dolomites (Rio Cordon catchment, Selva di Cadore, Belluno) in North Eastern Italian Alps, in Veneto region. (Figure 2.1)

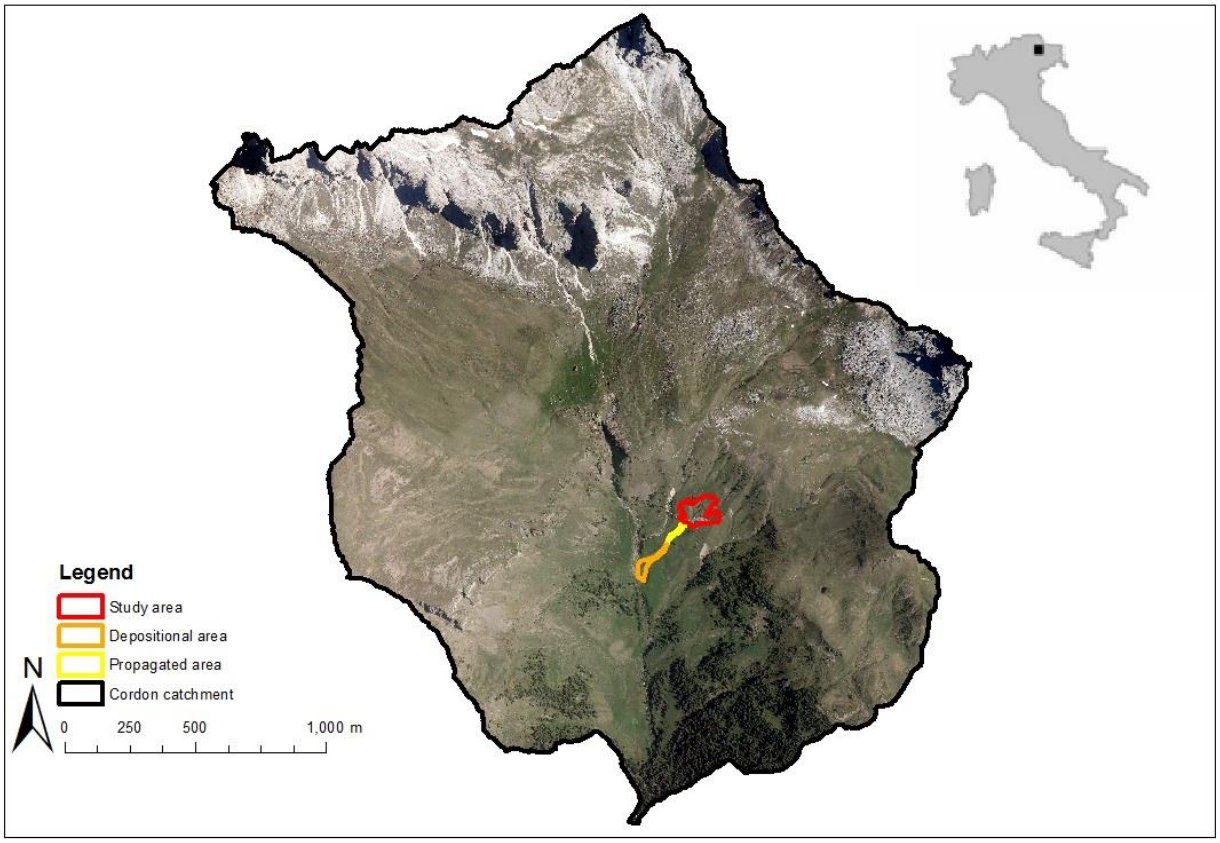

Figure 2.1 Cordon catchment and its position in Italy. It is also possible to identify the study area divided into landslide area (red), propagation area (yellow) and deposition area (orange)

2.1 THE RIO CORDON CATCHMENT

The Rio Cordon catchment is one of the most studied headwater basin in Dolomites (Bossi et al. 2015; Bovo 2012; Cavalli et al. 2008, 2016; Ferrato et al. n.d.; Rainato et al. 2016) because of the presence of a bed load and suspended load monitoring system since 1985 (Marchi et al, 1992) (Figure 2.1). The low anthropization makes the catchment a suitable study site for several researches since this aspect permits to preserve catchment's natural environment and observe natural processes with low interferences by human infrastructure. The human interference in this area can be summed up in:

(i) a seasonal passage of tourists on two hiking paths, (ii) a cattle grazing during summer, and (iii) the presence of two alpine summer houses (Malga Mondeval superiore e Malga Mondeval inferiore).
The Cordon stream is an III° degree tributary of Fiorentina creek that in its turn flows into the Cordevole torrent.
The outlet of Rio Cordon is placed to the confluence with the Fiorentina creek and it drains 7.68 km^2 (Bovo, 2012). The monitoring station is placed at 1763 m.a.l.s. and the upslope area is 5 km^2 (Cavalli et al, 2016). All the following data reported in this chapter refer to the Rio Cordon upslope area with an outlet section placed to the monitoring station (basin of 5 Km^2).

Figure 2.2 Sediment monitoring station of Cordon catchment, Credits Righetto 2011

The elevation ranges from 1763 to 2748 m.a.s.l. and the average slope is 27°. (Cavalli et al, 2016)
Climate conditions are typical of Alpine environments with a mean annual rainfall around 1100 mm, most of this precipitation occurs in form of snowfall from November to April. (Cavalli et al, 2016)
From May to August it is registered the highest frequency of precipitations of the year with rain peak about 150 mm and flood events happens in three different period of the year (Bovo, 2012):

- Flood events between May and June are due to snow melt (Marchi et al, 1992);
- Flood events between July and August are probably caused by high magnitude precipitations which are registered in this period;
- During September and October events characterized by high magnitude and frequency are registered. They can be very dangerous in a small catchment like Cordon catchment.

The sediment budget of the Rio Cordon, equipped for bed load monitoring since 1985, seems to be characterized by floods with a high magnitude and a low frequency (Rainato et al, 2016). The most severe flood recorded at the Rio Cordon monitoring station occurred in 1994.
The channel bed of the Rio Cordon is mainly composed by pebble and rocks and the typical morphologies are step-pool and cascade.
The vegetation cover is typical of temperate mountainous area and it consists mainly of mountain grassland (61%) and the 18% consists in widespread shrubs, while forest stands (spruce and larch) occupy 7% of the total area in the lower part of the catchment and the remaining percentage (14%) is bare land (Rainato et al, 2016).
Small groups of Alnus Virdis were observed also close to the channel bed of the Rio Cordon and its main tributaries. (Bovo, 2012)
The geological setting of the basin is characterized by dolomite rocks cropping out in the upper part and volcanic conglomerates, sandstones and calcareous-marly rocks dominating the middle and lower parts. Quaternary deposits (moraines, scree deposits, and landslide accumulations) are also common.
The morphology of this catchment is so diverse that is possible to divide it into three different parts based on morphological aspects (Marchi et al, 1992):

- High part "Spiz de Mondeval-Beco di Mezodì": is the highest part of the basin (Figure 2.3) easy to identify due to the exposed rock and cliffs of Lastoi, Punta de Ambrizola and de Beco di Mezzodì. The main lithotype is dolomites rocks and quaternary coverage is composed by a large amount of debris dolomites rocks due to landslide and debris flow that overlap with rocks of Wengen group;
- Middle part "Mondeval de Sora": this part of the basin has a low average slope and looks more flat except the oriental part of Monte di Mondeval. The lithology is composed by tuff and sandstone of the Wengen group. Quaternary coverage is heterogeneous and it is composed from very fine sand (loam, clay, and sand) to debris material. There are sediments instability on the surface layer, but there are also stabilized landslide partially covered by herbal vegetation, composed by dolomites debris rocks;
- Low part "Mondeval de Sote": this area there is characterized by a continuous evolution caused by the fluvial dynamics. In this area there are tuff and sand stone of the Wegen group and it is possible to find calcar and tiff stone of the Buchenstein group close to the outlet. The quaternary coverage is a part of the Wegen group and the Buchenstein group. Some amass of debris and some components of debris flow are visible.

Figure 2.3 from left to right-hand side of the picture of Loschiesuoi mountain, Forcella Giau, Formin mountain and Lastoi di Formin, Forcella Rossa, Ambrizzola peak, Forcella da Lago and Becco di Mezzodì mountain.

2.2 STUDY AREA

The sediment source area object of this study is placed on the hydrologic left part of Cordon catchment, in the Rio Col Duro sub-basin (Figures 2.1 and 2.4).

The study area was interested by a landslide due to snow melting during 2001. This event was composed by the collapse of different parts of the hillslope area. Then the landslide evolved in a mud flow that run along the hillslope and arrived in the Cordon stream, this event produced impacts in solid transport of the basin and changer in an evident way the morphology of this part of the Cordon catchment. The object of this thesis is not the entire event, but the study of the head part of the sub-basin, so only the first part of the event: the landslide part because only for this area we have a multi-temporal-high resolution database. The study area is visible in Figure 2.4 and is characterized by red color.

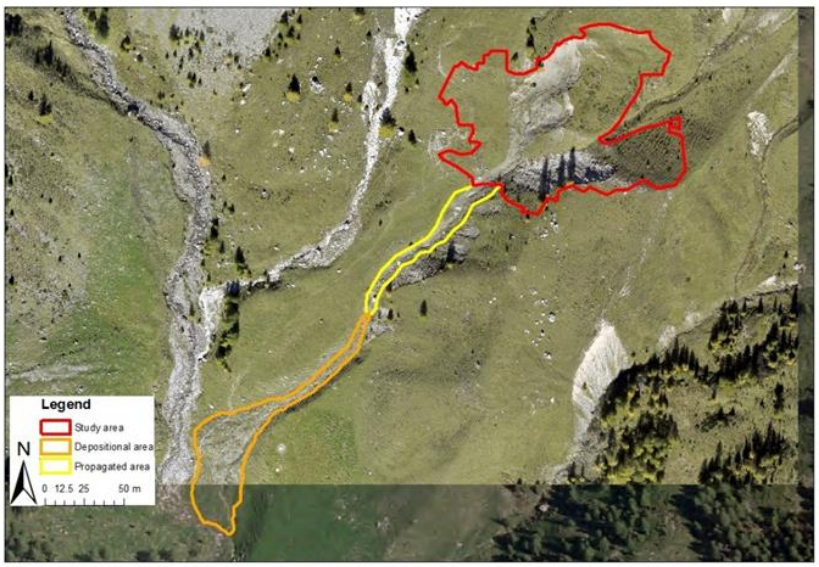

Figure 2.4 ortophoto of the study area, the landslide (red), the propagation area (yellow), and the depositional area (orange)

This area is placed between 2010 and 1800 m.a.l.s.

It is characterized by a landslide with a surface of 11750 m^2, a propagation area of 1063 $m^{2,}$ and a depositional area of 2900 m^2 (Figure 2.4) with slopes between 0° and 50° (Figure 2.5)

This area is characterized by an absence of arboreal vegetation: there are only some larches, spruces, and renewal of spruce. The rest of the area is exposed debris rocks or grass coverage.

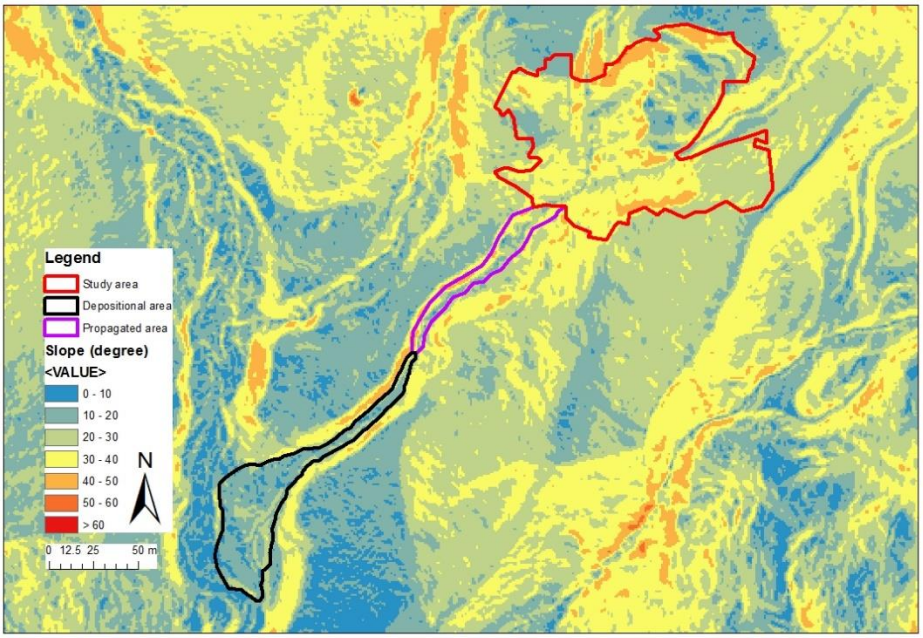

Figure 2.5 map of slopes (degree) the landslide area (red), the propagation area (viola), and the depositional area (black)

In this thesis will be analyzed only the landslide part because only for this area it is possible to obtain multi-temporal data.

For further photographs and information about the study area, reading the first part of Chapter 4 is recommended. In this chapter is possible to find a multi-temporal description of the area and related pictures.

3. MATERIALS AND METHODS

This thesis analyzes data collected using different remote sensing approaches (photogrammetric and LiDAR), so it is deemed as necessary to dedicate a chapter to go deeper this topic.

3.1 REMOTE SENSING TECHNIQUES

Surface displacements can be calculated using remote-sensing methods like interferometry for radar data and image correlation for optical data (Delacourt et al, 2007). These methods were elaborated during the last centuries and applied to sensors as radar, cameras, terrestrial laser scanner, and Lidar technologies. During the last decades these methods were applied also to the landslide(e.g. Bossi et al, 2015; Derron and Jaboyedoff, 2010).

Several remote sensing techniques and instruments are available to collect morphological data of a sediment source. To simplify the presentation of each one technique, the following part of this chapter will be divided using two parameters: the different kind of wavelength (Figure 3.1) that it is used by each method (radar, infrared, and visible) and the position of recording data (ground based, air-borne, and space-borne).

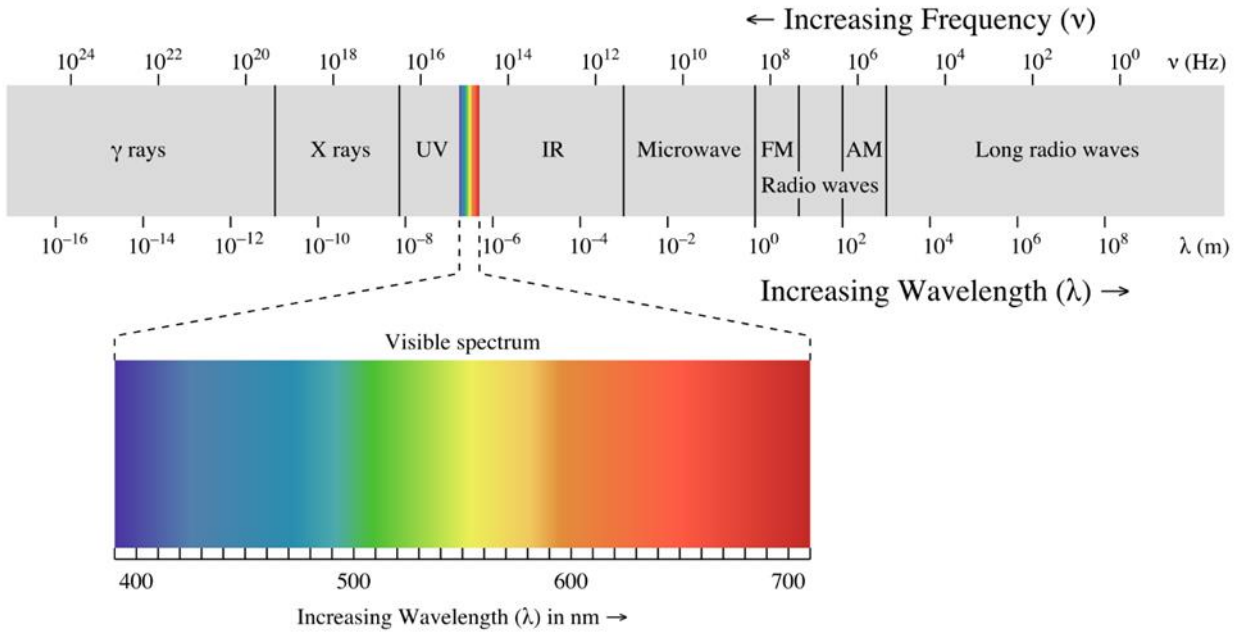

Figure 3.1 The electromagnetic spectrum extending from high to low frequencies. Optical sensor can cover the visible spectrum and LiDAR can cover from visible to near infrared region (NIR). Picture by Wikipedia.

3.1.1 RADAR REMOTE SENSING

InSAR (Interferometric Synthetic Aperture **Radar**) approaches are usually **ground-based** (Stow 1996; Tarchi et al, 2003) or **satellite-based** (Colesanti and Wasowski, 2006; Singhroy, 2009) and they rarely are **airborne**. InSAR approaches are mainly dedicated to the detection and the quantification of small displacements over large areas (Jaboyedoff, 2012). In this thesis it will not use radar data.

3.1.2 LIGHT DETECTION AND RANGING LiDAR (GROUND AND AIRBORNE)

LiDAR is the acronym for Light Imaging Detection And Ranging. It is an active sensor which uses visible IR and SWIR waves. It measures the distance between the platform and the point of wave rebound comparing the waves emission time with the following wave. So, the result of survey is a point cloud that can be used to monitor changes (Gordon et al, 2001) or to map (Ardizzone et al, 2007; Jaboyedoff et al, 2008) landslides and deformations. It is an active sensor and it does not depend on sun as light source; therefore, it is possible to carry out a survey all day long and in any season.
This sensor can detect and geo-localize objects with a high accuracy producing a high density point cloud. The density mainly depends on the position and the angulation of the sensor compared to the surveyed area and it can present from metric to decimetric resolution for airborne laser scanning (ALS) and from centimetric to millimetric resolution for terrestrial laser scanning (TLS) (Jaboyedoff et al, 2012; Shan and Toth 2008). With this technique it is possible to obtain a high-resolution DTM (Digital Terrain Model) and, at the same time, a high-resolution DSM (Digital Surface Model). The DTM is made of the bare ground data acquired by filtering vegetation and man-made features points (e.g. buildings) from the raw data (Cavalli and Tarolli 2011). A DSM is a digital model of surface obtained from LiDAR data characterized by the absence of any filtering processes (Cavalli and Tarolli, 2011); as a result, it is possible to study, not only surfaces, but also bare earth ground. This characteristic allows to conduct volumetric studies about vegetation. This instrument can be ground based or airborne.

The **Terrestrial** LiDAR Scanning (TLS) (Figure 3.2) is a ground based technique and it has a big potential in monitoring sediment source and landslides areas. Several researches use this instrument

to study landslides obtaining a high DEMs resolution (Jaboyedoff et al, 2010; Monserrat and Crosetto 2008; Schürch et al, 2011; Teza et al, 2007).

TLS survey is limited by the short ranges due to the wavelength used by the scanner. The most important limitations of the ground-based technique are the presence of shadow areas caused by rugged topography, the huge quantity of acquired information and the needed post-processing techniques for the filtering and the alignment of data sets, i.e. when a large area is scanned, several data sets must be merged and due to error propagation the alignment started to be more complicated and time-consuming to obtain reliable results (Jaboyedoff et al, 2012). These scanners are highly portable and not limited by changing weather conditions during surveys because of their wave-length. A big disadvantage of the system is the pricing. TLS systems with SLR (Single-lens Reflex) camera, GPS unit and software are expensive. Moreover, the range of the LiDAR system limits measurement areas to single slopes (Eckerstorfer et al, 2016). In comparison with Aerial Laser Scanner, TLS has more limitation in range and areal coverage.

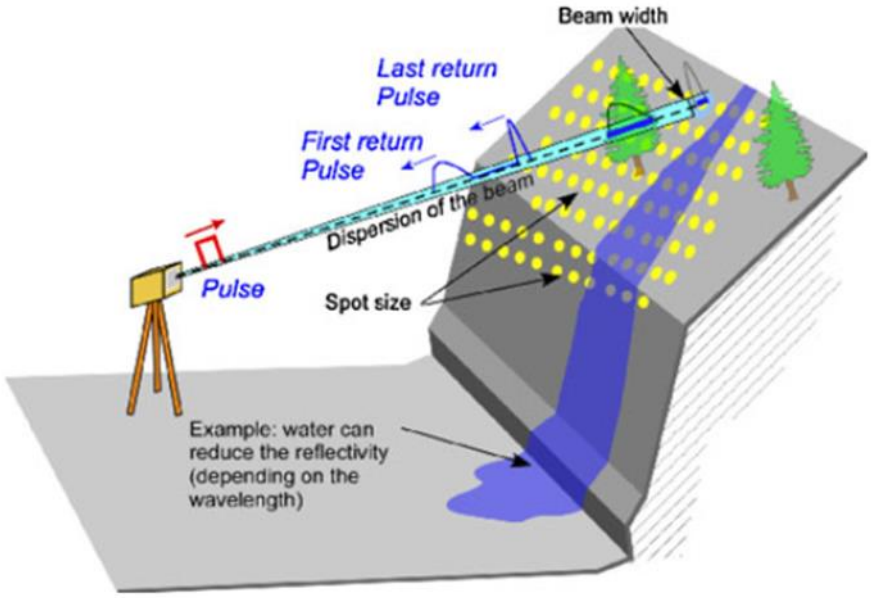

Figure 3.2 Laser scanner data acquisition, a TLS example (figure credits: (Jaboyedoff et al, 2012)*)*

About **aerial** LiDAR remote sensing, there are basically two type of ALS (Aerial Laser Scanner): the helicopter-based and the aircraft-based. The first one, in comparison with the second one, can give a higher resolution and allows to orientate the scanner in all directions (Vallet and Skaloud 2004).

Compared to TLS, the ALS technique is less flexible and accurate in particular for steep areas monitoring, where ALS incidence angle would lead to a low point of density (Hodgson and Bresnahan 2004) and also costs are higher. However, this approach has a high potential in surveying studies because of its higher coverage capacity and its velocity.

In the last decade there Aerial LiDAR branch made a lot of improvements.

There are not LiDAR **space-borne** approach.

3.1.3 OPTICAL REMOTE SENSING OF LANDSLIDES

Electromagnetic properties of earth material are really useful for landslide detection and mapping. Analyzing the visual spectrum, it is possible to immediately see that material absorbs, reflects or scatters different kind of waves based on its characteristic and based on the orientation of the object. Differences between two areas based on change of colors and brightness are immediately visible.

One of the most famous **ground based** approach is time-lapse photography (Eckerstorfer, 2016). This method allows to continuously monitor active landslides. The image monitoring system consists of a high-resolution optical camera installed on a concrete pillar placed on a stable crest in front of the landslide and controlled by a data logger (Travelletti et al, 2012). This method is also used to complete dataset of landslides inventories (e.g. Cavalli et al, 2016). The interval usually is between 1 and 10 years, but it can be also shorter in some active areas. This approach is very low-cost, but in some situations it is possible that the operator cannot take a picture from the same position. Seeing all the differences between pictures can be difficult in this situation.
It is also possible to use optical imagery to reproduce three dimensional surfaces based on photogrammetry principle. The last discovery in photogrammetry sector is the Structure from Motion (SfM) technique (Koenderink and van Doorn, 1991) This argument will be explored fully in Chapter 3.2.

Airborne based optical remote sensing tools are useful devices and there are many natural hazard studies based on aerial optical images.
In late 1990s, stereoscopic air-photo interpretation was still the most frequent remote sensing tool applied in mapping and monitoring of landslides (Metternichtet al, 2005) and also nowadays it is a good instrument in association with topographic maps and field surveys. The advantage of this technique is that it allows to book a flight survey whenever it is needed and for a specific area; the disadvantages are that this technique is influenced by the weather, it is not a low cost method, and images need to be processed to reduce geometric distortions.
A recently developed system has provided new opportunities for photogrammetric applications which is UAV (Unmanned Aerial Vehicles). UAV is a really promising aerial platforms, especially for landslides studies, where it is possible to apply photographic technology and other technologies. The

UAV has demonstrated its capability for producing topographic data on landslide areas which are usually not easy to reach. More improvements are required to reduce data processing time for the efficient generation of ortho-mosaics based on photogrammetric DTMs, in order to minimize georeferencing errors (Niethammer et al. 2011). This sector is expanding also in SfM applications.

Space borne based tools can produce data from low to high-resolution and they are used in huge number of natural science studies (e.g. landslide, flood, and fire mapping). Optical space borne images are an important support to understand changes during time of a landslide. They are really useful because satellites can cover with high frequencies the same surfaces. It currently exists a good assortment of high-resolution satellites and, for example, QuikBird has a spatial resolution of 0.6m in the panchromatic channel (2.4 m for multispectral bands). Nowadays almost all the satellites data are not free and datasets are not low-cost, but, since 2013, Landsat-8 provides free high-resolution optical data worldwide. In the panchromatic channel the spatial resolution is 15 m over a swath of 100×100 km (Eckerstrofer, 2016). However, it is not possible to acquire a satellite covering for a specific moment. Now ESA is working on a mission called "Sentinel-2 mission" to reduce this disadvantage. It is a land monitoring constellation of two satellites that provides high-resolution optical imagery, continuity for the current SPOT and Landsat missions. (www.earth.esa.int). The aim of the mission is to cover the land surface of earth completely every 5 days making the datasets free. The first sentinel (Sentinel-2A) was launched in 23 June 2015 and the launch of the second one (Sentinel-2B) is planned in 2017.

3.2 SfM APPROACH

Structure from Motion (SfM) is a recent technique for the production of high quality Digital Surface Models (DSMs). This technique is based on photogrammetric method: it uses images acquired from multiple viewpoints to produce a 3d high-resolution model of the subject surface. SfM uses also Ground Control Points (GCPs) or GCP of camera position and its angulation (Fonstad et al, 2013) as key points to understand the real position of each pixel and to estimate errors.
Some of the most interesting aspects of SfM are the very low costs in terms of capital and labor and the ease of use (Fonstad et al, 2013) in comparison with LiDAR and with the radar elaboration data. This method has also a high level of automation during the steps of camera calibration analysis of pictures and creation of point cloud using Photoscan software.

The essential instruments that an operator needs to perform a SfM data collection are: a camera, a GPS, and some "high visible" targets. The higher the resolution of the camera and the precision of the GPS are, the lower the error will be (these aspects will be examined in depth in Chapter 3.4).
There is a huge number of programs doing photogrammetric interpolations (E.g. Photoscan and VisualSFM) which allow the creation of point cloud that can be processed with GIS software.
This method recently become really widespread and it was applied in many research fields like paleontology (Falkingham 2012), archeology (Green et al, 2014; Verhoeven, 2011), lava flow processes (James et al, 2012), and gully erosion assessment (Castillo et al, 2012).

As already mentioned in previous chapter (Chapter 3.1.3), SfM is not only a ground based technique, but it can be also air-based; several studies demonstrated the usefulness of UAVs and light aircraft applied to SfM technique. Some examples are those of studies on mudslide (Niethammer et al, 2010), glacier (Welty et al, 2010), and avalanche (Eckerstorfer et al, 2016). Especially in the latter case, the application was performed in really dangerous environments where risks for the staff can be reduced significantly using UAV system.

3.3 DoD

DEM of Difference (DoD) shows variations of elevation between a sequence of DEMs of the same area. Basically it allows to quantify the amount of erosion and deposition throughout time; so, if high-resolution DTMs before and after the event are available, it is possible to estimate the mobilized sediment (Cavalli et al, 2015). Each DTM is affected by uncertainties and it is fundamental to consider them within the analysis. To facilitate DoD analysis, a software named Geomorphic Change Detection (GCD) has been developed based on existing methods and on the method by Wheaton et al (2010). More details can be found in Chapter 3.4.
This ArcGIS plugin was developed for morphological sediment budgeting analysis in rivers (http://gcd.joewheaton.org/). Several studies investigated multi-temporal analysis and applied DoD approach (Blasone et al, 2014; Bossi et al, 2015; Cavalli et al, 2015; Prosdocimi et al, 2015).

3.4 MATERIALS, DATA AND SOFTWARE

Datasets of the Cordon catchment were analyzed to study morphology evolutions of the study area between 2006 and 2016. Several topographic surveys have been carried out since 2006 to cover

Cordon catchment or a part of it. There were used different techniques and covered different areal extensions throughout time in the Cordon catchment, thus the study area was analyzed three times: between 2006 and 2015 with high-resolution technologies, in 2006, in 2010, and in 2011. The available datasets were made by different tools:

- In October 2006 using a helicopter with ALTM 3100 OPTECH and Rollei H20 Digital camera. The helicopter was flying at an altitude of 1000 m above ground level covering the entire catchment. So, using LiDAR technology it was generated a Digital Terrain Model (DTM) 0.5 m resolution (Cavalli et al, 2008). Unfortunately, instead of a point cloud, it was only available a 0.5 m DTM. Finally, it was produced a point cloud using ArcGis by means of "raster to point" tool. The point cloud had 4 points/m^2;
- In 2010, using an aerial LiDAR technology to cover all the surfaces of Dolomites by UNESCO because Dolomites have been declared a UNESCO World hermitage in 2009. The point cloud had 4 points/m^2;
- Another survey was done between 4th and 6th October 2011, using a Riegl® LMS-Z620 TLS system (Terrestrial Laser Scanner) for a project of University of Padua to cover only a face of Rio Cordon catchment using four scan position. A Digital Terrain Model (DTM) was generated with 0.1 m resolution. This survey covered only the study area and a part of the propagation area. Also in this case the point cloud was not available: only the 0.1 m DTM raster dataset was provided. So, it was produced a point cloud using ArcGis using "raster to point" tool. Have a point cloud is fundamental to make the point clouds co-registration. Without this passage the produced DoD is not reliable. The point cloud had 10 points/m^2.

To analyze the morphological evolution of study area throughout the time, the point clouds in 2006, in 2010, and in 2011 derived by these three different datasets were used. In addition, in 15th July 2016 a SfM analysis was done on the study area to obtain a high-resolution and recent cloud of the study area.

We structured the SfM analysis placing 18 targets inside the study area and collecting the GPS position of those targets. Then we started to take pictures of the study area following the procedure required by Photoscan (the program that we used to create the point cloud from photos which is presented below). Pictures were taken making a circle around the study area avoiding to keep two pictures from the same place. Some of them were also taken crossing the central section of the landslide taking picture in each side. Picture were also taken in the central part because of the complexity of the study area morphology. At least one target was included in each picture.

To collect data in the field, the following instruments were used:

- Rtk station to collect the raw GPS position of our targets (with a margin of error around 2-3 meters); these coordinates were processed by Cirgeo using ephemeris data from Borca di Cadore station to obtain an error around 2-3 cm (for more information visit http://retegnssveneto.cisas.unipd.it);
- Target (29.7 x 42.0 cm) to identify the position of each GPS known coordinate, detected using the rtk station;
- Panasonic DMC-FZ1000 was used as camera to take pictures of the study area.

The available data were analyzed with the DoD approach which is explained below in Chapter 3.5.3.

For this thesis were used four software: **ConVe, Photoscan, CloudCompare,** and **Arcgis**.
At the beginning ConVe program was used. It is a program produced by Veneto region, in order to convert coordinates into different systems and it is particularly suitable for way-points collected in Veneto region. We use it to convert ellipsoid gps point into geodetic points.

Photoscan 1.2 by Agisoft was used to create the point cloud of 2016.
This is a program produced to perform a photogrammetric processing of digital photo. Photoscan can create 3D models through a photo process using a semiautomatic approach:

- Pictures are uploaded in Photoscan;
- The first time every target is inserted manually and then the program stats to recognize targets automatically; so, the technician needs only to control each target in every picture to be sure that they are in the right position. Moreover, he has to change position of targets (if it is needed) because of some shift errors due to the automatic process;
- Then GPS positions of targets can be uploaded and the shift error between the reality and the reconstruction of the 3D can be automatically calculated by the program;
- If the shift error is admissible, the point cloud can be exported as a text file (e.g. ".txt" or ".xyz") or in the most suitable format for this operation. Then it is possible to continue the flow of the elaboration process.

It is really important following some rules during the collection of pictures in the field, if people want to work with Photoscan software. These recommendations are also reported in Photoscan Handbook

(http://www.agisoft.com). If these easy rules will not be followed, it is not possible to have a good starting dataset and the elaboration will be incorrect or rough:

- The digital camera should have an appropriate high-resolution, 5 MPix or more to allow the production of a high point cloud reproduction;
- It is important to use the same camera model for each survey area;
- The recommended focal length is 50 mm and 35 mm film equivalent. It is important to avoid fisheye lenses and ultra-wide angle; otherwise, in the first step there would be some aberrations around the outline. In addition, this would change the positions of part of the objects and there would be alteration in the point cloud;
- Take the same focal length and not zoom in or out during the data collection; otherwise, the dimension of pixels would change during the experiment and, as a result, the correlation between the dimension of pixels and the distance of the object to the point of view would be lost. This correlation allows the fundamental computation of distance between places where the pictures were taken and the object;
- Do not take two or more pictures from the same position, it is sufficient doing few steps to have enough degrees to allow the photogrammetric process (Figure 3.3);
- In case of aerial photography, the overlap requirement can be put in the following figures: 60% of side overlap + 80% of forward overlap;
- If it is possible, prefer cloudy days to avoid strong shadows that can make impossible to see areas that are under-exposed;
- Using pictures made by the same camera at the same zoom and knowing the exact position of some targets allow to place each pixel that appears at least in two figures in the space and to recreate the original shape of objects, buildings, and terrain.

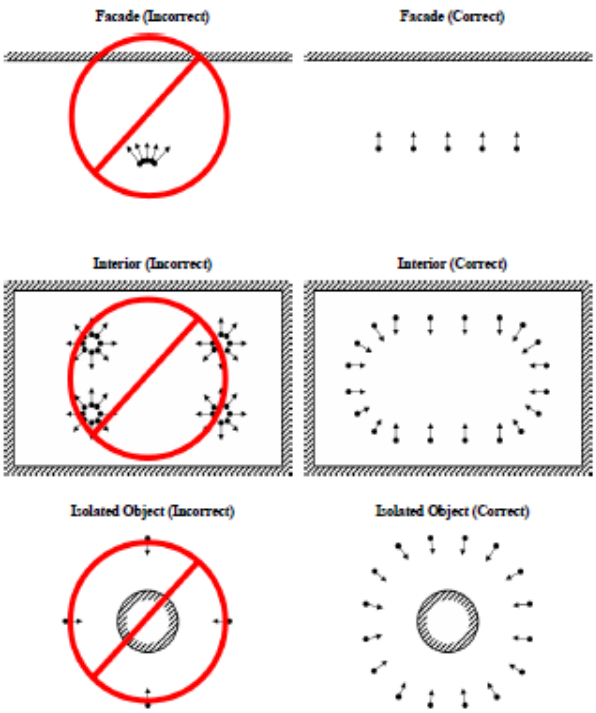

Figure 3.3 examples of corrects way to take picture of a subject (Credits to www.agisoft.com)

Another essential software for developing of this thesis is **CloudCompare 2.7.0** which is an open source software used to process 3D point clouds. It is a real versatile software that allow to modify, to compare two or more point clouds and to make some statistic computations. For example, it is possible to divide a point cloud or merge it with another and to shift it using a matrix or manually. It allows also to overlap two or more point clouds using different procedures (e.g. Fine registration (ICP) or point picking) and to make some analysis like standard deviation, mean distance or RMS.
This program was used to clean the point cloud of 2016 from incorrect points and trees and to make the co-registration between stable areas. This aspect will be explained in the following chapter.
The disadvantage of using this software to analyze changes in a certain area is that CloudCompare was born to compare or overlap two (or more) clouds of a steady area. So, it presents some difficulties to overlap areas which are different in two clouds. It tries to find a perfect match between these two surfaces changing completely the position and orientation of the cloud. This means that the clouds will not overlap also in the cases in which the area was steady.

ArcGIS is the last, but not least used program in this thesis. It is a professional Geographic Information System (GIS), developed by ESRI®. It was used to process geo-referred data, to convert them from point clouds into a DTM, to create a DEM of Difference (DoD) using CGD tool, to make maps, and to visualize ortophoto.

3.5 METHODS

It is possible to summarize the analysis carried out into four different phases:

- Data collection;
- SfM survey and point clouds elaboration;
- Co-registration of each point clouds;
- DoD production and analysis.

3.5.1 DATA COLLECTION

Cordon catchment was selected as possible study area based on the availability of a big multi-temporal database including a TLS (Terrestrial Laser Scanner) dataset of the landslide chosen as a study area. Then topographic data were provided by the TeSAF department.
For further information about used datasets check Chapter 3.4.

3.5.2 SfM SURVEY AND POINT CLOUDS ELABORATION

A topographic survey was conducted on July 15th in order to have a DTM conducted in 2016 comparing previous DTMs with a recent one. In the field we used a rtk station, 18 targets, and a camera.
We placed the rtk reference station in an upper position compared to the study area and chose a place without elements that could disturb the signal between reference and rover like trees or hills.
18 targets were placed in the whole study area to make sure to cover all the surface and that all the markers should have another marker in a range around 10-15 meters.
Pictures were taken using the precaution reported in the previous part of the Chapter 3.4.

Pictures were elaborated in Photoscan and blurred pictures were deleted. 143 pictures were chosen to build a point cloud. Using a proper tool (workflow → align pictures), they were aligned and the not aligned pictures were deleted. Then Targets were signed in each picture, but, at the beginning, adding targets manually is necessary and then the program starts to recognize automatically targets position; therefore, the technician needs only to check if the position is right. GPS positions of marker were added and the ranges of errors were controlled.

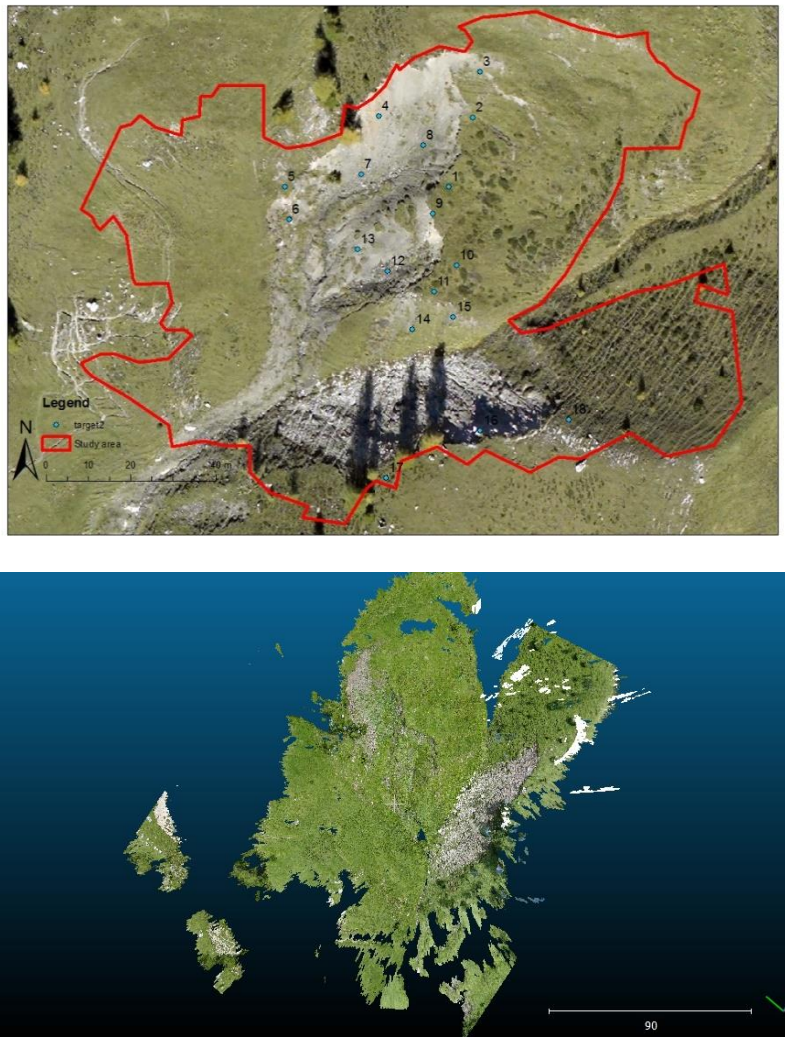

Figure 3.4 above the study area and the position of the targets, below the raw point cloud made by Photoscan

Different attempts were made at different resolutions and with diverse combinations. Finally, we decided to use the high resolution and 5 markers (targets n 5-6-8-13-16). An error of 0.21 m as position error was obtained with this combination.

When the most suitable target combination was chosen, a cloud was build using "build a dense cloud" tool placed in "workflow". Different point clouds were produced changing resolution parameters and then the high resolution was chosen. We chose a point cloud with the following characteristics after different attempts:

- Numbers of points 44 775 889
- Error between points 0.19m
- targets used (targets n 5-6-8-13-16) (Figure 3.4)

This step can require even two days to a computer with 16GB of ram to be processed, if it is used "dense" (high) as resolution. But in this way it is possible to create a detailed point cloud with almost 45.000.000 points.

Then points were exported and written in a ".txt" format.

When a satisfying 3D model was created, the point cloud was processed using CloudCompare to cancel points that could add errors during the DTM creation because the original point cloud encompasses vegetation, points outside of the study area, and non-existent pixels created for a wrong interpolation made by software (e.g the white points showed in Figure 3.4). Thus, filtering out these features was necessary to obtain a new point cloud representative of bare earth ground (Figure 3.5).

The new cloud had the following characteristics:

- 43 160 629 points
- Minimum number of points: 0 p/m^2
- Maximum number of points: 18 802 p/m^2
- Mean number of points: 3 434 p/m^2

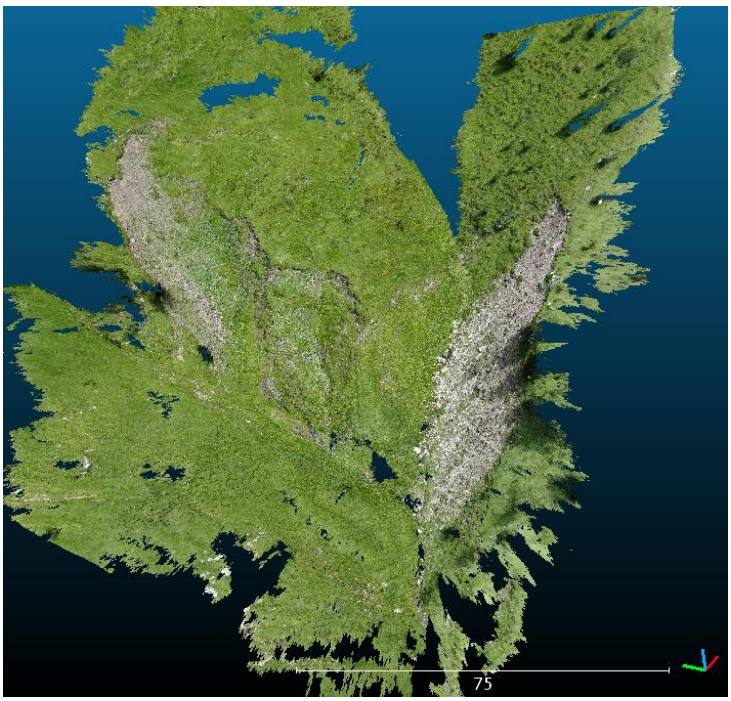

Figure 3.5 the clean point cloud, visualized in CloudCompare

Then it was converted into a text file (".txt") and uploaded on ArcGis to create Digital Terrain Models of the study area at different resolutions (0.05m, 0.1m, 0.2m, 0.5m, 1.) making a first analysis and being sure that the file was exploitable.

Data were imported in ArcGis using the following procedure (**first procedure**):

- The point cloud was saved using a text format ".txt";
- It was uploaded in ArcGIS using "add data" and fields "x", "y", and "z" were checked;
- Finally, an event-shape file was created using "feature to 3D by attribute".

This procedure failed only with this point cloud (2016 point cloud) causing a crash of ArcGIS every time. It was probably caused by the large amount of data contained in the file. However, it did not fail with the other clouds and it was applied to clouds "2006", "2010", and "2011" because there were less passages and there were consequentially less possibilities to add errors.
So, the following procedure was used for the data from 2016 (**second procedure**):

- The point cloud was saved using a text format ".xyz ";
- A Geodatabase file and a feature dataset (inside the geodatabase) were created;
- The point cloud file ".xyz" was converted using "from file to point file information" tool (3D Analyst Tools → Conversion → From File → Point file information). Decimal point was selected as "decimal spacing" and the value was written down in order to do the following steps;
- The cloud was converted using "ASCII 3D to feature class" tool (3D Analyst tools → Conversion → From File → ASCII 3D to feature class). It was selected "Multipoint" in "feature class" field and the point spacing number found above in the "point spacing" field;
- The feature class was imported in ArcGIS and a terrain was created. A DTM 0.5 was built using "Terrain to raster" tool. (ArcToolBox → 3D Analyst Tools → Conversion → From Terrain → Terrain to raster).

3.5.3 CO-REGISTRATION

All the four landslide datasets were uploaded in Arcgis. The 2006 dataset was projected in ellipsoidal coordinate system using Monte Mario datum, whereas the other datasets were projected using geoidal coordinates system using WGS84 datum; therefore, there was an altitude difference of 50 meters between the 2006 dataset and the others. Arcgis was used to reduce the vertical distance shifting the 2006 landslide point cloud of 50 meters following the z axis. Lessening the vertical distance between

clouds, the effort that CloudCompare needs to overlap different clouds and the resulting error are reduced.

Each shade of hill was studied to find some stable areas for making the co-registration possible.

Three stable areas were found in each dataset and exported as point clouds in CloudCompare. Each pair of stable areas was aligned creating a matrix using fine registration (ICP) tool (Figure 3.3). The reference cloud was considered the one of 2011 because it was made by a technology more reliable and accurate than the others; in addition, we had more information about data than the others. In the case in which there was not the 2011 cloud in the pair of clouds that were co-registered, we tried both the clouds as reference and we chose the attempt with the best result in the DoD step.

The co-registration step was done to overlap almost perfectly one cloud with the others before performing DoD analysis. It allows to reduce topographic vector uncertainty (xδ, yδ, and zδ)

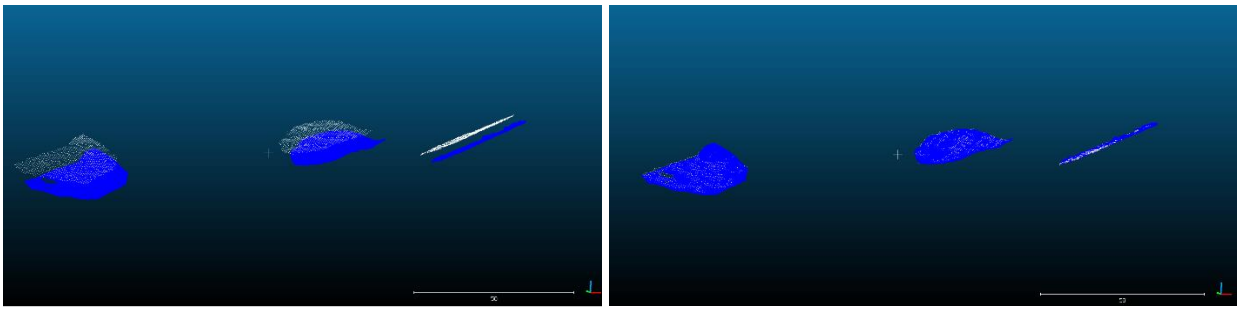

Figure 3.6 Before (left) and after (right) a co-registration of three sable areas, using ICP tool

Statistical parameters were also calculated for each pair of co-registered stable areas like standard deviation, mean distance and final RMS. Different attempts of selection of stable areas extension were done for each comparison, in order to find the low deviation standard and the most accurate result was chosen. Then the matrix was applied to the entire point cloud and the overlapping was checked. These statistical analyses were applied to control the quality of data and to quantify uncertainty (δz) within DoD (Wheaton et al, 2010).

3.5.4 DoD COMPUTATION AND ANALYSIS

An analysis of the shade of the hill was made in ArcGIS for each DTM raster obtained from point clouds to avoid errors caused by the “natural neighbors” process which is used to create each DTM. This happens because in a point cloud we have punctual information and, when we want to produce a DTM, it is necessary to convert a punctual information into an information that covers all the areas of the surface. To make this transformation, in this thesis “natural neighbors” conversion technique

is applied to the point cloud to produce a DTM raster: we use the interpolation between the closest known points to this area to understand the value of unknown points. In two cases, if there are no points for an entire area of a point cloud or if the density point is not enough for a specific area of a point cloud, there is a high probability that the transformation is not representative of the data for these areas, especially if the represented area is placed in a heterogeneous environment like a mountainous area. This is a problem if the purpose of the study is analyzing the differences of amount of mass. For this reason, it is important to avoid those areas during the computation. To identify those areas, the hillshade shape of each surface was analyzed. Moreover, it is possible to identify those areas because raster is smooth on the hillside. The hillshade become smooth where there are not points or where the density point in not enough in a point cloud.

Then the common surface considered for each DTM was the one that had no problem caused by "natural neighbors ".

For each attempts a DoD was calculated using raster calculator to produce a rough DoD. So, it was possible to understand if the overlapping of clouds succeeded. In the following picture (Figure 3.6), it is possible to observe two DoDs examples: in each one the erosion is colored in red and the deposition is colored in blue. On the left side the computational error is clear: the erosion and the deposition area is too huge which means that there is a shift between two point clouds. On the right side there is a more plausible comparison: erosion and sedimentations are reduced and placed in reliable places.

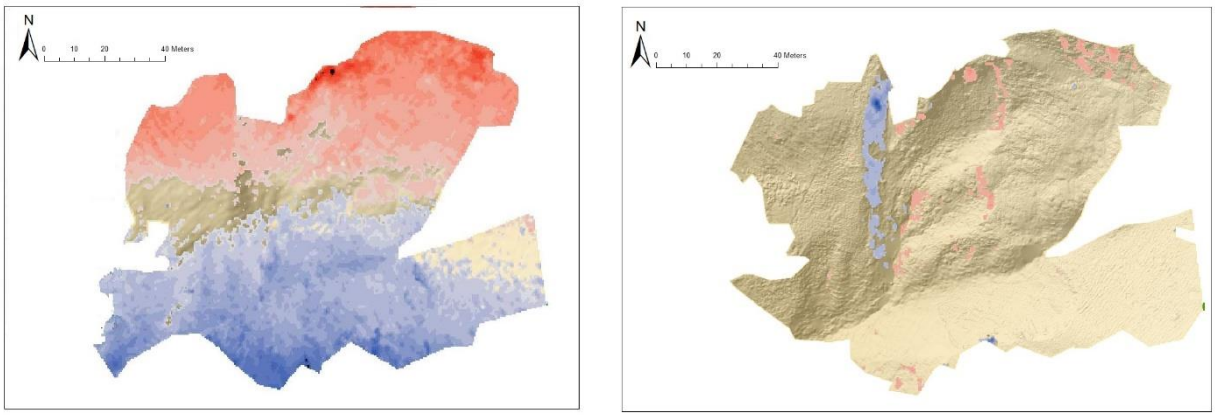

Figure 3.7 two examples of a DEMs of difference of the same study area. The first (left) is an example with a high shift error, on the right there is an example plausible right

When co-registration results were considered suitable, GCP tool was used for DoD computation using the deviation standard calculated between stables areas as minimum level of detection.

In fact, xδ and yδ uncertainties were considered negligible after the co-registration of point clouds and the altitude uncertainties were considered related to the actual altitude using the Wheaton (2010) approach:

$$Z_{Actual} = Z_{DEM} \pm \delta z \quad (1)$$

In this kind of approach the real value of elevation is Z_{Actual} and Z_{DEM} is the elevation reported in the DTM cells.

zδ includes manufacturer reported precision, measurement errors, sampling bias (density and sampling patterns), and interpolation methods (Wheaton et al, 2010).

DEM uncertainty can be transferred and propagated into the DoD as explained by the following formula (Brasington et al, 2003):

$$\delta u_{DoD} = \sqrt{(\delta z_{new})^2 + (\delta z_{old})^2} \quad (2)$$

while the propagated error in DoD is δu_{DoD}, the individual error of the new DEM is δz_{new} and the individual error of the old DEM is δz_{old}

So, the propagated DoD uncertainty is reasonable approximating to SDE (standard deviation of error) (Wheaton, 2010). In this case SDE was calculated during the stable area co-registration.

Co-registration and DoD steps are “try and error processes”, thus we tried and tried again to find the most suitable result.

4. RESULTS

An historical photo-analysis was carried out to identify areas with visible changes during the last 15 years (2001-2016). Pictures of the area were taken in 2001 immediately after the event, in 2006, in 2010, and in 2011. This dataset was updated with pictures taken during the 2016 field survey. It was possible to have an overview of the historical evolution of the study area through this analysis.
Not all photographs were taken from the same point of view, but most of the study area was covered except for some images gap of 2006, 2010, and 2011 for some parts of the landslide. In the pictures below, it is presented:

- A picture with an overview of the entire interested area by the 2001 event throughout time (Figure 4.1) with a gap for year 2011;
- A picture with a comparison between 2011 and 2016 eroded area (Figure 4.2);
- A picture representing the right-hand hillslope side of the study area (Figure 4.3), in which the 2010 picture is missing;
- In Figure 4.4, in 2006, in 2010 and in 2016 the downstream part of the landslide is missing, but all the triggering area is represented;
- A picture representing the left hand hillslope side of the study area (Figure 4.5), in which the 2001 the left-hand slope is missing.

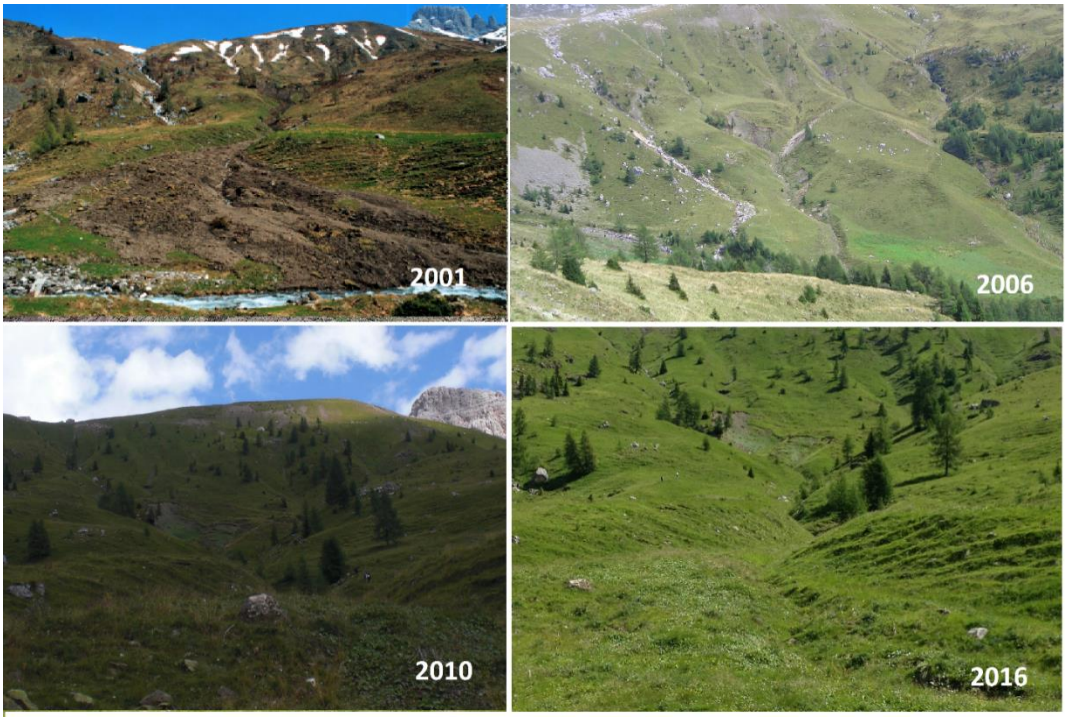

Figure 4.1 picture of the study area from 2001 (credits to Lorenzo Marchi), 2006 (credits to Marco Cavalli), 2010 (credits to Vitali) and 2016 (credits to Jesssica De Marco)

In Figure 4.1 it is possible to observe the evolution of the study area during the last 15 years. A progressive stabilization of the mud flow deposit and the landslide propagation area are evident in the lowest part of the interested area by the event occurred in 2001.

By comparing pictures taken in different years, it is possible to perform a visual analysis of evolution through time of the landslide: in Figure 4.2, two active erosions are identified in two pictures of 2011 and 2016 on the right-hand side of the main landslide unit. The left-hand side was not considered for images comparison since there were not significant changes.

In the picture of 2016 in comparison with 2011 landslide (Figures 4.3 and 4.4), it is possible to observe that there is a new covering of grass vegetation in the low and central part of the right-hand side.

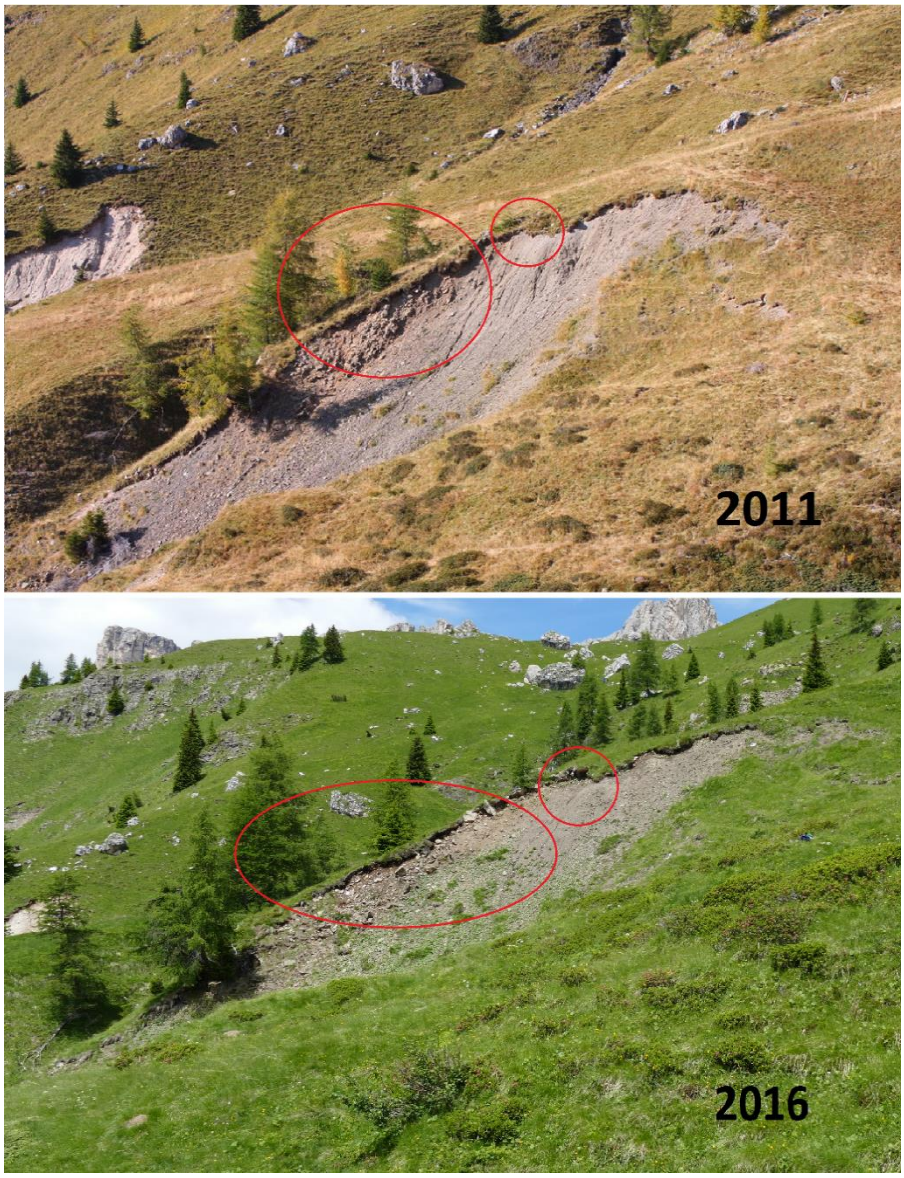

Figure 4.2 visible changes between 2011(credits to Righetto) and 2016 (credits to Jessica De Marco)

In this section there are reported photographs from different periods of the same parts of the study area: in Figure 4.3 the high right-hand side of the landslide is shown, while in Figure 4.4 the low right side is shown and Figure 4.5 shows the high left side of the landslide.

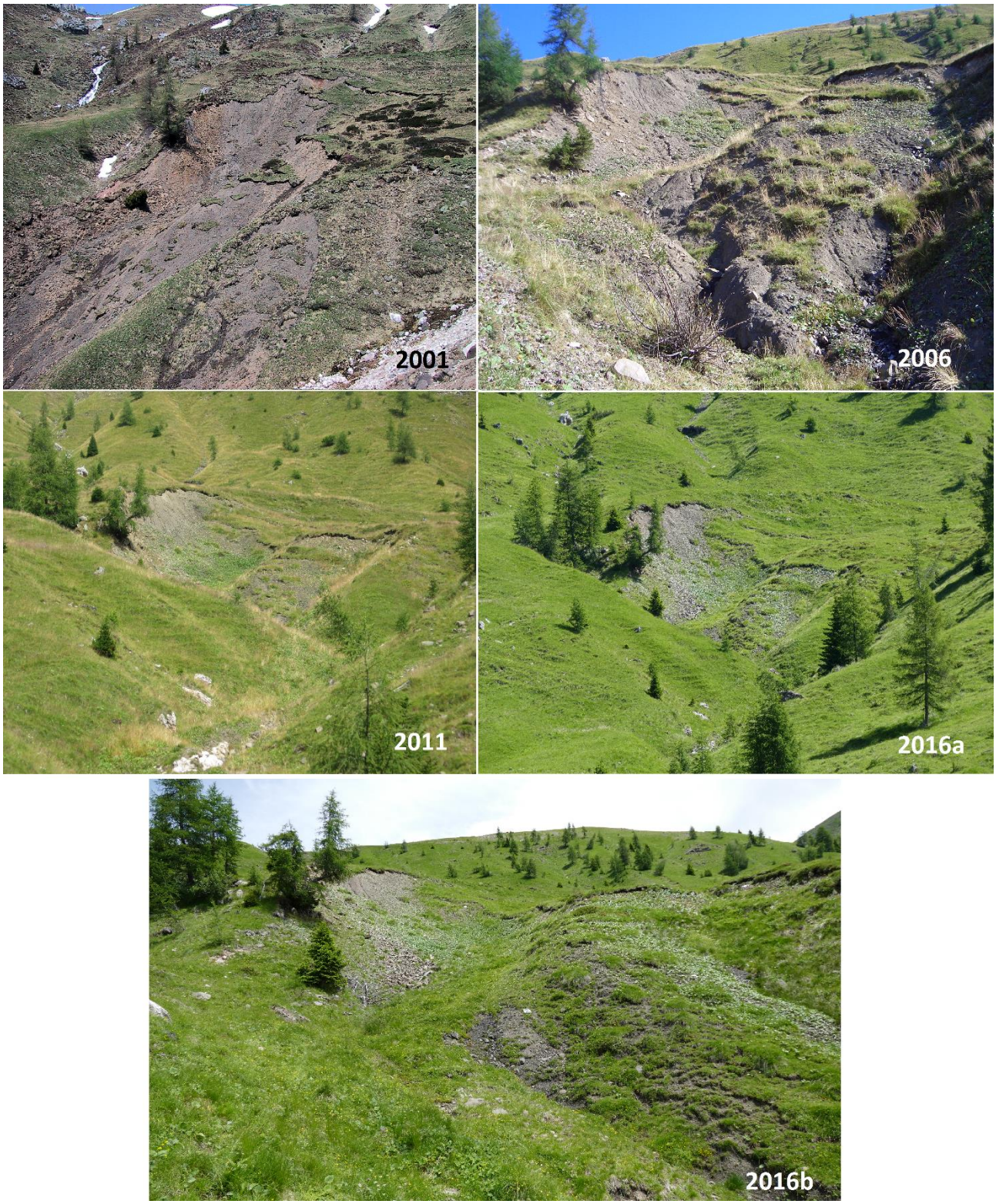

Figure 4.3 photo of the right-hand part of the study area from 2001 (credit to Lorenzo Marchi) 2006 (credits to Marco Cavalli), 2011(credits to Calligaro), and 2016 (a and b) (credits to Jessica De Marco)

From the observation of Figure 4.3, it is evident that the landslide crown has been interested by erosion processes since 2001. A grass vegetation cover grew between 2006 and 2016 and no mass movements are visible in other parts of the interested area by these pictures. In the low part of 2016b photo there are still parts which are not covered by grass; therefore, it suggests that erosion processes are still active.

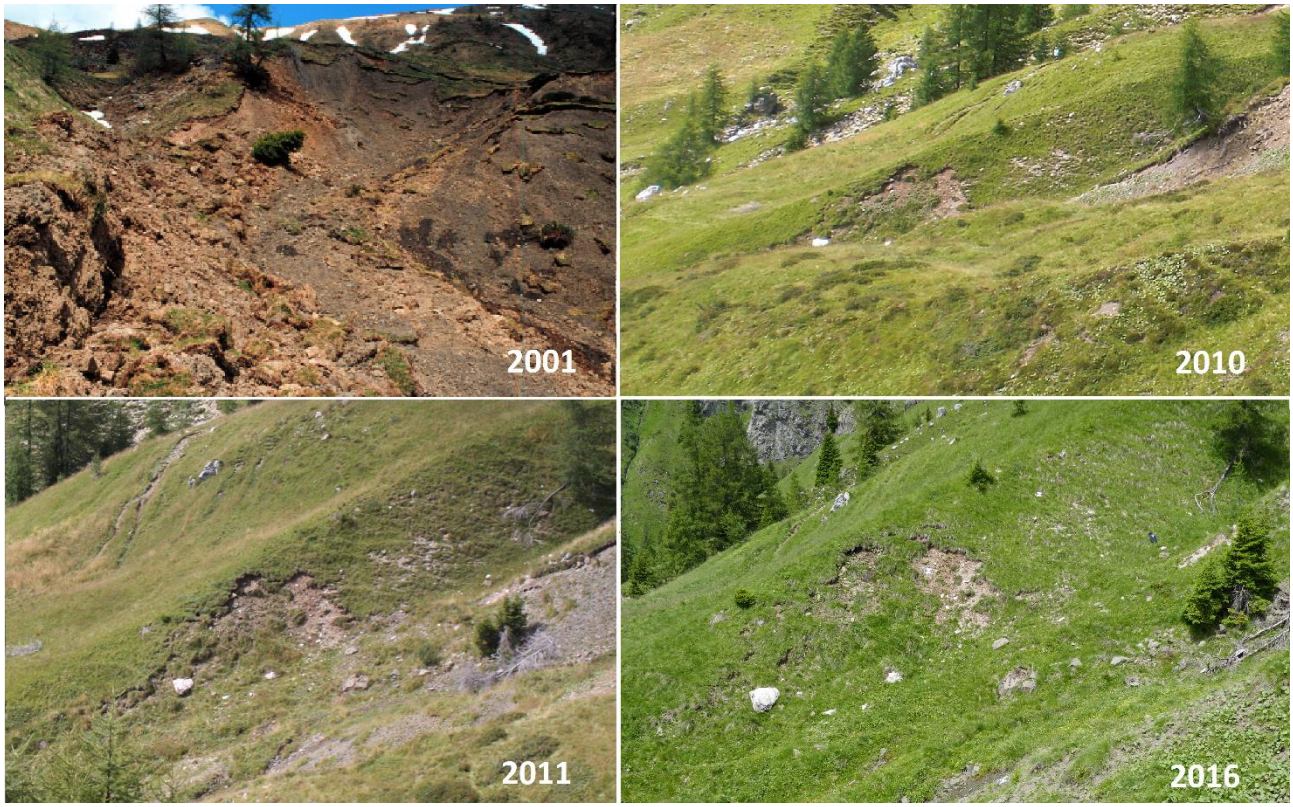

Figure 4.4 photo of the right-low part of the study area from 2001 (credit to Lorenzo Marchi) 2010 (credits to Vitali), 2011(credits to Righetto) and 2016 (credits to Jessica De Marco)

From the observation of Figure 4.4, it is possible to see a high growth of grass vegetation between 2001 and 2010. Unfortunately, there are not pictures from 2006 about this part of the study area, so it is not possible to know if the covering occurred before or after 2006. We can suppose looking at Figure 4.3 that vegetation growth started before 2006.

Figure 4.5 photo of the left side of the study area from 2001 (a and b)(credit to Lorenzo Marchi), 2011(credits to Righetto) and 2016 (a and b) (credits to Jessica De Marco)

Also in Figure 4.5 there is not a photo of 2006 because it was not found a picture concerning the study area and 2001 photos are partially hide; however, no evident changes are visible between 2011 and 2016 and also the rocks seem to be still in the same position.

These picture will be mentioned also later.

4.1 DOD ANALYSIS

Six groups of DoD were produced in order to compare each point cloud with the others and to understand the evolution of the sediment source throughout time. This is an advantage to monitor also one result with the others. DoDs groups are:

- 2016-2006
- 2016-2010
- 2016-2011
- 2011-2006
- 2011-2010
- 2010-2006

In order to compare the different DTMs derived throughout the years, we need to accurately co-register point clouds. For this reason, we decided to align the point clouds based on matrix derived from the co-registration of stable areas because, as already mentioned in in previous chapter (Chapter 3.4), it is important to use stable areas to correctly make the co-registration; otherwise, it is not possible to overlap clouds in CloudCompare.
A lot of attempts were made to find the right combination of stable areas (Figure 4.8):

1. One stable area chose between a1, a2 or a3;
2. Two stable areas chose between a1, a2, and a3;
3. Two stable areas a1 and a4 where a4 is a part of the landslide that in the picture seems to be stable;
4. Three stable areas a1, a2, and a3.

The fourth combination showed the most suitable results, so the parameters derived from this analysis were used to align the point clouds.

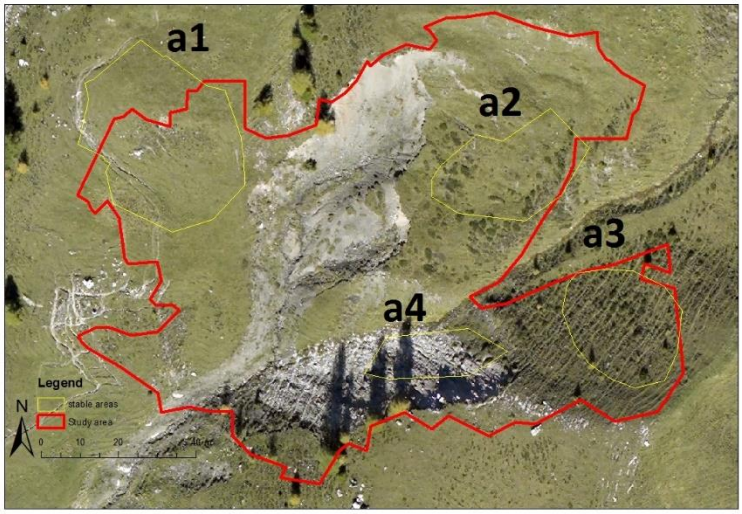

Figure 4.6: stable areas used during different attempts to make co-registration

Clouds had different extensions and not all the points cover exactly the entire surfaces. Moreover, they had different surfaces characterized by "natural neighbour" problems (for further details, see Chapter 3.5.3). So, the most suitable extents of stable areas were chosen for each pair of clouds.

The pairs of stable areas were aligned using the most accurate cloud of the pair was used as model/reference and the other one was compared to the first one, so we obtained a matrix which applied in a rigid transformation to the whole study area point cloud. The statistical parameters obtained in the co-registration of the stable areas are reported in Table 4.1.

Different attempts of selection of stable areas extension were done for each comparison, in order to find the low deviation standard and the most accurate result was chosen.

Table 4.1 statistical characteristics of each DoD comparison

DoD	Standard deviation error	Mean distance	Root mean square
2016 – 2006	0.10	0.25	0.27
2016 – 2010	0.21	0.12	0.29
2016 – 2011	0.17	0.27	0.32
2011 – 2006	0.76	0.57	0.95
2011 – 2010	0.28	0.35	0.45
2010 – 2006	0.46	0.33	0.57

The standard deviation of stable areas derived from the co-registration was used as threshold to distinguish between real changes and changes due to uncertainty.

The obtained DoD results are reported in the following subsection.

DoD 2011-2006

To make this DEM of Differences (Figure 4.6), the matrix was applied to point cloud 2006 and the 2011 point cloud was used as reference; then the point clouds were converted into raster with 0.5 m size cell and the DoD was calculated using GCD Arcgis plugin. The DoD map (Figure 4.3) shows a reliable pattern of geomorphic changes: an erosion area is evident in the northern-eastern part of the study area. A pattern of deposition can be observed in the northern-central part which occurred most likely between 2006 and 2010 as suggested by the growth of grass vegetation in that area between 2001 and 2010. This was also presented by the comparative analysis. (Figure 4.4).

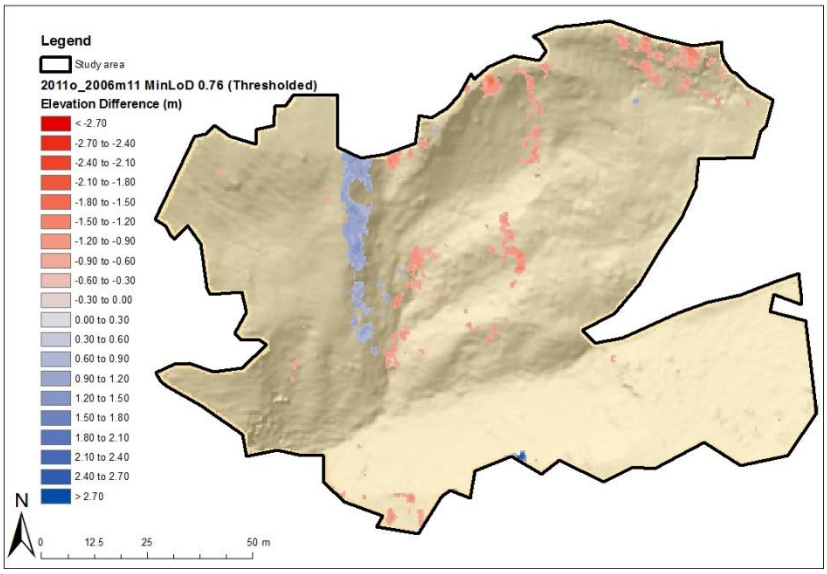

Figure 4.7 DoD map for the period 2006-201. The blue parts are characterized by deposition and the red parts are characterized by erosion

There is a small area in the lower part of the DoD characterized by a deposition of 2.9 meters. This feature of the map is due to a tree. It was recognized as bare ground in 2011 by the TLS, but the Lidar made in 2006 did not detect it; as a result, in the DoD this area looks like a deposition of mass. This problem is present also in others DoD in 2011 (e.g. DoD 2011-2010 and DoD 2016-2011 in which the area was represented in the DoD as erosional). This error appears also in other areas of the clouds, but they were outside of the study area.

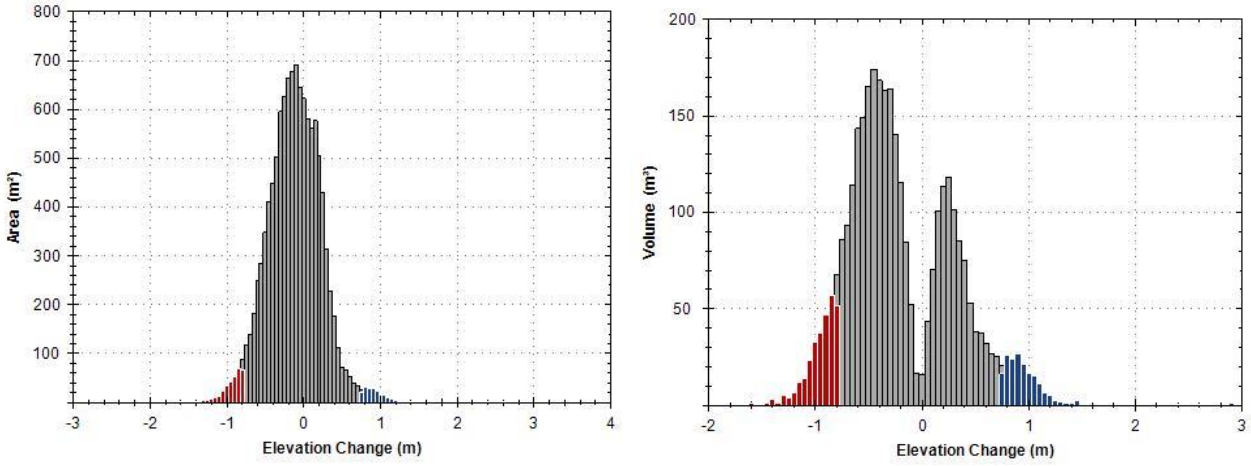

Figure 4.8Histogram of the area interested by erosion and deposition (left) in blue and red are marked the surfaces interested by deposition and erosion respectively using the threshold. Histogram of the volume interested by erosion and deposition (left) in blue and red are marked the volumes interested by deposition and erosion respectively using the threshold

The standard deviation error used as minimum level of detection in this DoD can be considered quite realistic because of the combination of some intrinsic factors of the 2006 point cloud.

Table 4.2 table of data about Dod 2011-2006

Attribute	Raw	Thresholded		± Error Vo	% Error
AREAL:					
Total Area of Erosion (m²)	6,932.25	326.25			
Total Area of Deposition (m²)	4,564.75	188.50			
Total Area of Detectable Change (m²)	NA	514.75			
Total Area of Interest (m²)	11,497.00	NA			
Percent of Area of Interest with Detectable Change	NA	4.48%			
VOLUMETRIC:					
Total Volume of Erosion (m³)	2,141.91	296.36	±	247.95	83.66
Total Volume of Deposition (m³)	1,122.78	182.71	±	143.26	78.41
Total Volume of Difference (m³)	3,264.69	479.08	±	391.21	81.66
Total Net Volume Difference (m³)	-1,019.12	-113.65	±	286.36	-251.97
VERTICAL AVERAGES:					
Average Depth of Erosion (m)	0.31	0.91	±	0.76	83.66
Average Depth of Deposition (m)	0.25	0.97	±	0.76	78.41
Average Total Thickness of Difference (m) for Area of Interest	0.28	0.04	±	0.03	81.66
Average Net Thickness of Difference (m) for Area of Interest	-0.09	-0.01	±	0.02	-251.97
Average Total Thickness of Difference (m) for Area with Detectable Change	NA	0.93	±	0.76	81.66
Average Net Thickness of Difference (m) for Area with Detectable Change	NA	-0.22	±	0.56	-251.97
PERCENTAGES (BY VOLUME):					
Percent Erosion	65.61	61.86			
Percent Deposition	34.39	38.14			
Percent Imbalance (departure from equilibium)	-15.61	-11.86			
Net to Total Volume Ratio	-31.22	-23.72			

It is important to remember that the 2006 data were provided at the beginning of the study not like point clouds, but as raster format with a resolution of 0.5 m. So, the raster file was converted again into a point cloud to make the co-registration in CloudCompare. Finally, these data were not the

original point cloud, so they were less accurate that a point cloud. Moreover, it is possible to clearly see the slide made by the sensor analyzing the hillshade derived from 2006 raster data. This is an additional error that can increase the standard deviation error. This feature was visible in all the DoD based on 2006 cloud, except for DoD 2016-2006.

In Figure 4.7 two histograms are shown representing area (left) and volume (right) interested by erosion and deposition. The grey part is the area/volume interested by deposition and respectively erosion excluded from the final amount because considered under the threshold. In blue and red are marked the areas/volumes interested by deposition and erosion. Associating Figure 4.7 with data collected in Table 4.1, the use of the threshold is clear: for example, the total volume of difference between 2006 and 2011 DEM is 479.08 m^3 ±392.21 m^3 of error instead of 3264.69 m^3.

Looking at the data in Table 4.1, it is possible to observe that the total net volume difference is negative (-113.65 m^3) with an error of ± 286.36, suggesting that the study area between 2006 and 2011 featured quite active erosional processes.

The next results of maps and graphics will be reported as annex at the end of the thesis.

DoD 2016-2011

To make this DEM of Differences (Annex 2), the matrix was applied to point cloud 2016 and the 2011 point cloud was used as reference; then the point clouds were converted into raster. Two different attempts were made using the co-registered raster: (a) a DoD between two 0.5 raster resolution (b) a DoD between two 0.2 raster resolution. To do these different attempts, the same data were used with the same co-registration and basically the same co-registration was used to make different resolutions DoDs. Therefore, the statistical parameters are the same for both the attempts, so also the threshold (0.17 m) is the same.

For the first attempt (Annex 2a), an over estimation of the depositional area and of the thickness of deposition is visible in the map. The parts considered "depositional" were vegetated in 2011 and not covered by grass vegetation in 2001. The same active erosional parts of the DoD 2011-2006 are still visible in the northern part of the map.

Making a comparison between the 0.5 m DoD and the 0.2 m DoD (Attached 2a and 2b), it is possible to observe that raw values are lower in the first table than in the second one. This is due to cells resolution because using a higher resolution it is possible to analyze better the surface, the threshold and consequently the amount of mobilized sediment. These elements are also visible comparing histograms on the amount of area and volume interested by erosion and depositions. The 0.2 m DoD

is more accurate and its analysis resulted in lower amount of interested areas and volumes than the 0.5 m Dod.

DoD 2016-2006

To make this DEM of Differences (Annex 3), the matrix was applied to point cloud 2016 and the 2006 point cloud was used as reference; then the point clouds were converted into raster with 0.5 m size cell and then the DoD was calculated using GCD Arcgis plugin.
This DoD looks rough, but it was made of a low threshold (0.1 m) and some similarities with the previous Dods are evident: There is an erosion area in the northern part of the image and it is also visible the same deposition of 2006-2011 Dod (Attached 1) located in the northern-middle area. The rest of data are unclear and they are probably caused by the impossibility to have a best-match between point cloud 2006 and point cloud 2016. This is added to the characteristics of 2006 cloud already reported in the previous chapter "DoD 2011-2006"

DoD 2011-2010

To make this DEM of Differences (Annex 4), the matrix was applied to point cloud 2010 and the 2011 point cloud was used as reference; then the point clouds were converted into raster with 0.5 m size cell and then the DoD was calculated using GCD Arcgis plugin. There were made two attempts of co-registration and the second one was chosen because of a lower standard deviation and some better data characteristics; however, results are still not satisfactory.
In all the DoD made by 2010 cloud a high error of co-registration arose. Those errors are visible in the map of Annex 4. For example, the entire left-hand side of the slope is completely in deposition and also other large surfaces are completely characterized by depositions or erosions; therefore, this suggests that the best-match co-registration was not made. In addition, the range of deposition thickness is between 0 and 5 meters which is too high basing on the pictures analysis and the period of time covered by this DoD (one year). Unfortunately, the only part covered by pictures for this period is the low-right part. It is possible to observe in Figure 4.4 that no changes occurred between 2010 and 2011 for the low-right hand side of the landslide; however, this area looks as if there was an erosion in the map in Annex 4.

DoD 2010-2006

To make this DEM of Differences (Annex 5), the matrix was applied to point cloud 2006 and the 2010 point cloud was used as reference; then the point clouds were converted into raster with 0.5 m size cell and then the DoD was calculated using GCD Arcgis plugin. Also in this DoD map it is possible to observe errors due to the co-registrations and 2010 point cloud: the left-hand part of the landslide is in deposition and the other side in erosion. This DoD corresponds to 2011-2006 DoD because of the erosion located in the northern part of the landslide.
About the DoD map of 2010-2006, it is clearly visible a shift to the left of 2010 cloud in comparison with 2006 cloud. It is visible thanks to the location of the pattern of the erosion and accumulation.
The co-registration error is less evident in this DoD than in 2011-2010 DoD; for example, in this case the amount of interested areas by changes is less (10.16%) than in the previous DoD (80.37%). Data are more realistic in this case, but the error is still high.

DoD 2016-2010

To make this DEM of Differences (Annex 6), the matrix was applied to point cloud 2010 and the 2016 point cloud was used as reference; then the point clouds were converted into raster with 0.5 m size cell and then the DoD was calculated using GCD Arcgis plugin.
In this DoD high errors of co-registration can be observed and they are visible in the maps of the Annex 6. For example, the entire low part and the left-hand side of the study area are completely in deposition. In addition, also the high part is completely in erosion probably due to the impossibility to obtain a better co-registration. The erosion and deposition are probably caused by the shift which seems to create imperfect match between the two clouds as in DoD 2011-2010.

5. DISCUSSION

The main topic of this work is analyzing data acquired with different techniques. Several DoDs (See Annex and Chapter 4) were produced to understand the evolution of this sediment source area. The most realistic one (DoD 2006-2011) shows a localized erosion in the north-eastern part of the landslide and a deposition in the middle northern part of the study area during the period 2006-2011(Annex 1). This was confirmed by photographs collected throughout time (Figures 4.3 and 4.4). Looking at the data (Annex 1), it is evident that the area was characterized by the erosion during the period 2006-2011 (Annex 1) and the erosion process was still active in the upper part of the landslide during the period 2011-2016 (Annex 2). Another important element is that the low part of the study area started to be covered by grass since 2006 (Figure 4.3), but only from the picture taken in 2011 it is possible to see (partially) a good coverage (Figure 4.3) that interests the low and central-right part of the study area; for this part of study area is visible a deposition in DoD 2011-2016 (Annex 2) probably due to the grass coverage and to some sediment deposition. This means that a big part of the area is progressively stabilizing, thus this process is still developing and it has improved for the last 15 years.
From DoD 2006-2016 (Annex 3) some similarities are visible with DoD 2006-2011 and DoD 2011-2016.
Also a comparison between the same period of time (2016-2011) at different resolution was done to verify if changing resolution, the quality of the DoD changes (Annex 2A and 2B). Comparing the two annexes, it is visible that using a higher resolution is possible to obtain a higher data accuracy.

During the thesis elaboration some problematic aspects were faced. For example, the production and analysis of 2016 point cloud was particularly complicated due to the complex morphology of the area and the high resolution of the obtained point cloud. The complex morphology created some problems during the cloud production: there were areas not covered by points because they were hidden and not covered by pictures. To make possible a complete coverage of the study area, it is recommended to pay attention to areas such as the central area and the parts of the study area immediately outside of the crown. Pictures of these parts cannot be easily taken. For this reason, those areas need more attention during the data collection and it is necessary to put at least a target outside of the crown for having a better target coverage.
The second problem was due to the high resolution of the 2016 point cloud; as a result, the cloud was transferred from Cloud Compere to ArcGIS using a different and longer process (Chapter 3)

compared to the process used for the other clouds. So, a certain degree of error was probably added to the co-registration applying a longer method.

The main issue of this work was that the point cloud datasets were made by different techniques and produced by different sources. Each cloud had its uncertainties and problems, which combined with the uncertainties and problems of the other clouds, propagated a certain error and presented issues in the final DoD maps. This makes harder to find a DoD with a low level of uncertainty. For example, the 2010 point cloud was difficult to align with the other clouds; changing the position of stable areas or trying with different ones, it was not possible to obtain an acceptable DoD. In addition, information about data were not available for the 2010 point cloud and it was unknown how LiDAR data were elaborated. The 2006 point cloud showed itself as a reliable point cloud of the study area. The 2006 point cloud characteristics probably slightly influenced DoDs: this cloud was obtained in a raster 0.5 resolution, thus it was converted again into a point cloud to make the co-registration.

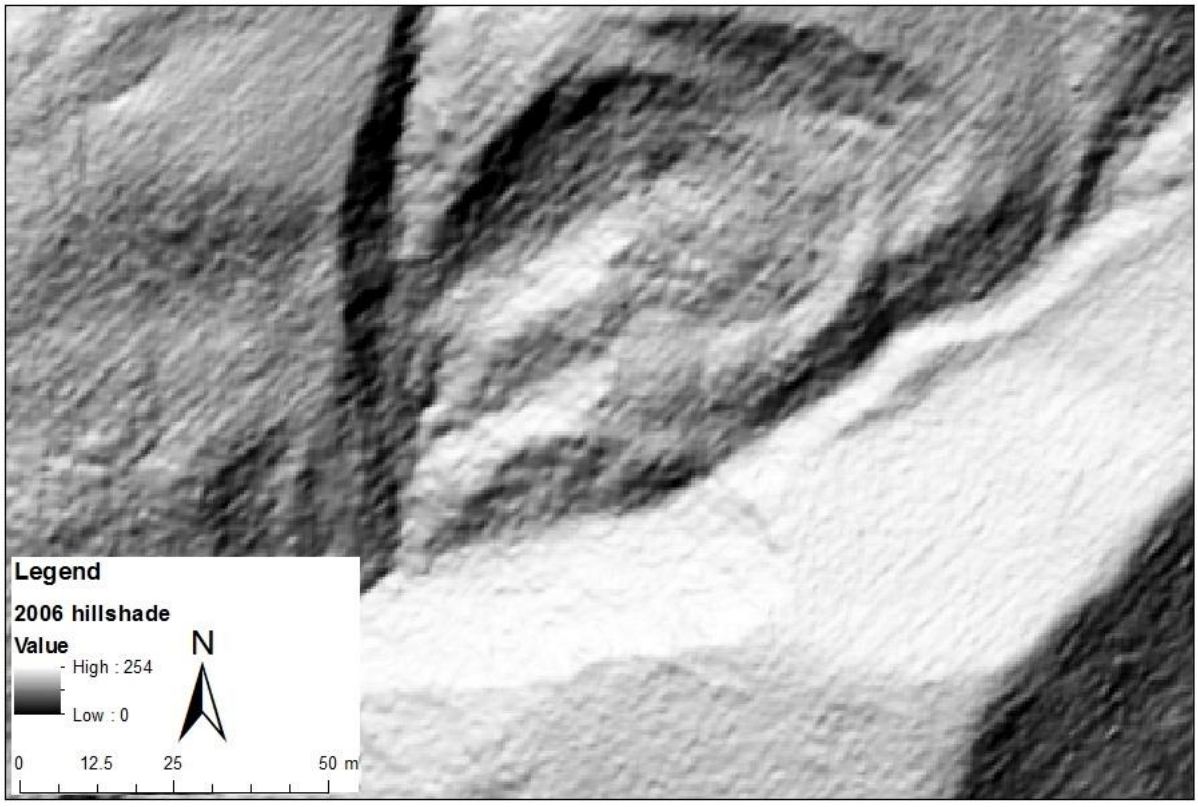

Figure 5.1 Hillshade o 2006 cloud point where the anomalies caused by the sensor are visible (lines with a north-eastern direction)

This transformation lowered the point density and this probably was one of the reasons of the high standard deviation in all the DoDs produced with the 2006 point cloud, except for the DoD 2006-2016. DoD 2006-2016 probably did not show this problem because of the imperfection of both point

clouds casually compensate out one to the other errors. Another characteristic of the 2006 cloud was the technologies used: the cloud is more than 10 years old, thus obtained by using an old Laser sensor that caused some anomalies in the data; slightly anomalies are visible only looking at the hillshade (Figure 5.1) and they look like lines, but a correlation between these anomalies and errors was not found.

The technologies were finalized to a DTM production and trees were filtered for cloud 2006, 2010, and 2016. The filtering process for 2006 and 2010 point clouds was done automatically by LiDAR tools using the bare ground points, while this process was done manually for 2016 point cloud (the one which was produced by SfM technique and there were no data collected due to the characteristics of the technique).

It is possible that in 2011 the filtering process was not perfectly done and some isolated tree remained in the DTM; as a result, this added some variables and errors to the DoDs (e.g. DoD 2010-2011 in the southern part of the map where it was visible an area with a deep erosion).

We dumped into another problematic aspect which was the nature of the program CloudCompare. The tool used to co-register each group of point cloud was created to perfectly overlap two or more clouds of the same area without changes. For this reason, the program tries to ideally overlap also in the case in which there are some changes. This can be a problem like in our case because the area is different in many points due to the environment and the events that happened throughout time. We have tried to reduce the problem using stable areas during the co-registration; however, co-registering them perfectly without errors is still hard.

Comparing point clouds produced using different techniques was possible to observe differences between the techniques used and their positive/negative aspects. In the case studied, the most reliable cloud was the 2011 point cloud which was produced using TLS technique. This cloud revealed itself as an accurate point cloud with a high point density, but elaborations were fast and without hitch. The only disadvantage by using this point cloud was the presence of some isolated trees inside the point cloud that changed the amount of erosion and deposition in DoD maps.

Also the 2006 cloud was well structured and data were reliable, the cloud was also well filtered and in the study area no trees were found. The disadvantage was related to the availability of only the DTM with cells of 0.5 meters and not of the original point cloud, this element made difficult to co-register accurately this point clouds with the others. Another disadvantage was interference of data caused by the sensor.

The 2016 point cloud was another interesting data because of its high resolution and its low cost production. There were problems concerning the co-registration probably due to some errors caused by the GPS position of targets, but the 2016-2011 and 2016-2006 DoDs showed interesting results

described in the previous chapter. This technique has high chances and probably in the next years this problem will probably be solved; as a result, it will be possible to have a best-match.
It was not possible to obtain reliable data with the 2010 point compared to the other clouds and there were not metadata information about this cloud (Chapter 3.4), thus it was not known exactly which technology was used, only that it was made by an ALS survey.

6. CONCLUSION

Our times are characterized by a high availability of data produced by different sources and by using different techniques. The main problem right now does not seem to be to obtain data, but it seems to be to compare data among themselves. This aspect is also visible in the case of geo-referred data. These data are produced through different techniques and acquired by different sources because these sensors are always in development. An actual and remarkable challenge is to gain the capability of producing reliable results through the comparison of data originated by using different methods.

In this thesis a multi-temporal analysis of a landslide during the last 10 years focused on the Rio Cordon Catchment (Belluno, Italy) was carried out in order to understand the evolution of the landslide area using high-resolution data derived from different data sources. LiDAR (ALS and TLS) and SfM technologies were used to produce those data sets.

Several digital elevation models comparison (DoDs) were produced to understand the evolution of this sediment source area. The most realistic one (DoD 2006-2011) shows localized erosion in the north-eastern part of the landslide and a deposition in the middle northern part of the study area during the period 2006-2011 (Annex 1). Another interesting result was obtained from DoD 2011-2016 that shows that there is still an active erosion in the northern part of the landslide instead there is a depositional area in the central and low part of the right-hand side of the landslide. From DoD 2006-2016 (Annex 3) some similarities are visible with DoD 2006-2011 and DoD 2011-2016.

This study offers the great opportunity of comparing high-resolution data in a low human impact area that allows to have a better understanding of the landslide area evolution after the 2001 triggering event and the application of SfM, a low cost technique which can produce a high density cloud.

Limitations were caused by the impossibility to perfectly overlap some point clouds (e.g point cloud 2010) with the others and by the difficulty to obtain a low uncertainty threshold (e.g. point cloud 2006). We tried to co-register the clouds using different stable areas extent, positions and numbers without obtaining better results. However, from this work it is evident that applying a “try and error” process is possible to at least understand which areas are interested by erosional and depositional processes. Looking at data, it is possible to say that the best technique to do this kind of survey seems to be the TLS immediately followed by the SfM which has big potentialities especially in terms of data quality and costs. However, with this SfM it is important to keep some advice in mind as pay attention to cover perfectly all the interested surfaces, remember that the area needs to be visible during the data collection (e.g. the bare ground should not be covered by trees) and pay attention to the GPS error. It is important to remember to pay attention in the field towards the issues which emerged in data collection for the 2016 cloud production. Trying to keep the target GPS points with

different tools can also be interesting to have a better understanding about GPS errors for different tools.

Continuing to produce point clouds of the study area using the SfM technique for further researches can be of relevant interest. Another aspect that deserve to be analyzed in depth is the evolution of sediment dynamics in the study area and how the rainfall and snow melting phenomena interact with the study area. It can also be interesting continue to produce 0.2 DoD resolution to have a better understanding of the sediment evolution.

REFERENCES

Ardizzone, F. et al. 2007. 'Identification and Mapping of Recent Rainfall-Induced Landslides Using Elevation Data Collected by Airborne Lidar'. *Nat Hazards Earth Syst Sci* 7: 637–650.

Blasone, Giacomo, Marco Cavalli, Lorenzo Marchi, and Federico Cazorzi. 2014. 'Monitoring Sediment Source Areas in a Debris-Flow Catchment Using Terrestrial Laser Scanning'. *Catena* 123: 23–36. http://dx.doi.org/10.1016/j.catena.2014.07.001.

Bossi, G. et al. 2015. 'Multi-Temporal LiDAR-DTMs as a Tool for Modelling a Complex Landslide: A Case Study in the Rotolon Catchment (Eastern Italian Alps)'. *Natural Hazards and Earth System Sciences* 15(4): 715–22.

Bovo, Nicola. 2012. 'Il Monitoraggio Del Trasporto Solido Di Fondo Nel Rio Cordon Tramite L'utilizzo Di Transponder Passivi'.

Bretar, F. et al. 2013. 'An Advanced Photogrammetricmethod Tomeasure Surface Roughness: Applica-Tion to Volcanic Terrains in the Piton de La Fournaise'. *Reunion Island. Remote Sens. Environ.* 135: 1–11.

Brunner, F., K. Macheiner, and H. Woschitz. 2007. 'Monitoring of Deep-Seated Mass Movements'. In *Proceedings of the Third International Conference on Structural Health Monitoring of Intelligent Infra-Structure (SHMII-3),* , 7p. (on CDROM).

Castillo, C. et al. 2012. 'Comparing the Accuracy of Several Field Methods for Mea- Suring Gully Erosion'. *Soil Sci. Soc. Am. J.*

Cavalli, Marco et al. 2015. 'Assessment of Erosion and Deposition in Steep Mountain Basins by Differencing Sequential Digital Terrain Models'. *Geomorphology* (2016). http://dx.doi.org/10.1016/j.geomorph.2016.04.009.

Cavalli, Marco, and Paolo Tarolli. 2011. 'Applicazione Della Tecnologia LIDAR Per Lo Studio Dei Corsi D'acqua'. *Italian Journal of Engineering Geology and Environment* 1(2011 SPECIALISSUE.1): 33–44.

Cavalli, Marco, Paolo Tarolli, Giancarlo Dalla Fontana, and Lorenzo Marchi. 2016. 'Multi-Temporal Analysis of Sediment Source Areas and Sediment Connectivity in the Rio Cordon Catchment (Dolomites)'. *Rendiconti Online Societa Geologica Italiana* 39: 27–30.

Cavalli, Marco, Paolo Tarolli, Lorenzo Marchi, and Giancarlo Dalla Fontana. 2008. 'The

Effectiveness of Airborne LiDAR Data in the Recognition of Channel-Bed Morphology'. *Catena* 73(3): 249–60.

Colesanti, Carlo, and Janusz Wasowski. 2006. 'Investigating Landslides with Space-Borne Synthetic Aperture Radar (SAR) Interferometry'. *Engineering Geology* 88(3–4): 173–99.

Cruden, D. M. 1991. 'A Simple Definition of a Landslide'. *Bulletin of the International Association of Engineering Geology* 43(1): 27–29.

Delacourt, C, P Allemand, E. Berthier, and Et Al. 2007. 'Remote-Sensing Techniques for Analysing Landslide Kinematics: A Review'. *Bulletin de la Socie´te´ Geologique de France*: 89–100.

Derron, M. H., and M. Jaboyedoff. 2010. 'LIDAR and DEM Techniques for Landslides Monitoring and Characterization'. *Natural Hazards and Earth System Science* 10(9): 1877–79.

Dietrich, W. E., D. Bellugi, and R. Real de Asua. 2001. 'Validation of the Shallow Landslide Model, SHALSTAB, for Forest Management'. *Wigmosta MS, Burges SJ (eds) Land use and watersheds: human influence on hydrology and geomorphology in urban and forest areas, Water Science and Application* 2.

Eckerstorfer, Markus, Yves Bühler, Regula Frauenfelder, and Eirik Malnes. 2016. 'Remote Sensing of Snow Avalanches: Recent Advances, Potential, and Limitations'. *Cold Regions Science and Technology* 121: 126–40. http://dx.doi.org/10.1016/j.coldregions.2015.11.001.

Falkingham, P. L. 2012. 'Acquisition of High resolution3Dmodels Using Free, Open-Source, Photogrammetric Software'. *Palaeontol. Electron.* 15 (1).

Ferrato, Caterina, Jessica De Marco, Paolo Tarolli, and Marco Cavalli. 'An Updated Sediment Source Areas Inventory in the Rio Cordon Catchment (Dolomites)'.

Fischer, W.A., W.R. Hemphill, and A. Kover. 1976. 'Progress in Remote Sensing (1972-1976)'. *Photogrammetria* 32: 33–72.

Fonstad, Mark A et al. 2013. 'Topographic Structure from Motion : A New Development in Photogrammetric Measurement'. 430(January): 421–30.

Foppe, K., W. Barth, and S. Preis. 2006. 'Autonomous Permanent Automatic Monitoring System with Robot-Tacheometers.' In *XXIII International FIG Congress 'Shaping the Change' (FIG-2006)*, , 12p. (on CDROM).

Gómez-Gutiérrez, Á., S. Schnabel, F. Berenguer-Sempere, F., Lavado-Contador, and J. Rubio-

Delgado. 2014. ‘Using 3D Photo-Reconstruction Methods to Estimate Gully Headcut Erosion.’ *Catena* 120: 91–101.

Gordon, S., D. Lichti, and M. Stewart. 2001. ‘Application of a High-Resolution, Ground-Based Laser Scanner for Deformation Measurements’. In *Proceedings of the 10th International FIG Symposium on Deformation Measurements*, Orange, California, USA, 23–32.

Green, Susie, Andrew Bevan, and Michael Shapland. 2014. ‘A Comparative Assessment of Structure from Motion Methods for Archaeological Research’. *Journal of Archaeological Science* 46: 173–81. http://dx.doi.org/10.1016/j.jas.2014.02.030.

Guzzetti, Fausto et al. 2012. ‘Landslide Inventory Maps: New Tools for an Old Problem’. *Earth-Science Reviews* 112(1–2): 42–66. http://dx.doi.org/10.1016/j.earscirev.2012.02.001.

Highland, Lynn M, and Peter Bobrowsky. 2008. ‘The Landslide Handbook — A Guide to Understanding Landslides’. *Landslides*: 129.

Hodgson, M.E., and P. Bresnahan. 2004. ‘Accuracy of Airborne Lidar-Derived Elevation: Empir-Ical Assessment and Error Budget’. 70 (3): 331–339.

Jaboyedoff, M. et al. 2008. ‘Preliminary Slope Mass Movements Susceptibility Mapping Using LIDAR DEM’. In *Proceedings of 61th Canadian Geotechnical Conference, ,* 419–426.

———. 2010. ‘Use of LiDAR in Landslide Investigations: A Review’. *Nat. Hazards*: 1–24.

Jaboyedoff, M., P. Ornstein, and J.-D. Rouiller. 2004. ‘Design of a Geodetic Database and Associated Tools for Monitoring Rock-Slope Movements: The Example of the Top of Randa Rockfall Scar’. *Natural Hazards and Earth System Science* 4: 187–196.

Jaboyedoff, Michel et al. 2012. ‘Use of LIDAR in Landslide Investigations: A Review’. *Natural Hazards* 61(1): 5–28.

James, M. R., L. J. Applegarth, and H. Pinkerton. 2012. ‘Lava Channel Roof- Ing, Overflows, Breaches and Switching: Insights from the 2008–2009 Eruption of Mt. Etna’. *Bull. Volcanol.* 74: 107–17.

James, M.R., and N. Varley. 2012. ‘Identification of Structural Controls in an Active Lava Dome with High Resolution DEMs: Volcán de Colima, Mexico’. *Geophys. Res. Lett.* 39.

James, M R, and S Robson. 2012. ‘Straightforward Reconstruction of 3D Surfaces and Topography with a Camera : Accuracy and Geoscience Application’. 117(November 2011): 1–17.

Javernick, L, J Brasington, and B Caruso. 2014. 'Geomorphology Modeling the Topography of Shallow Braided Rivers Using Structure-from-Motion Photogrammetry'. *Geomorphology* 213: 166–82. http://dx.doi.org/10.1016/j.geomorph.2014.01.006.

Kääb, A., L. Girod, and I. Berthling. 2013. 'Surface Kinematics of Periglacial Sorted Circles Using Structure-from-Motion Technology'. *Cryosphere Discuss.* 7: 6043–6074.

Kasperski, Johan et al. 2010. 'Application of a Terrestrial Laser Scanner (TLS) to the Study of the Séchilienne Landslide (Isère, France)'. *Remote Sensing* 2(12): 2785–2802.

Koenderink, J.J., and A.J. van Doorn. 1991. 'Affine Structure from Motion, J'. *Optical Soc. of America A* 8(2): 337–85.

Lichti, D.D., and S. Jamtsho. 2006. 'Angular Resolution of Terrestrial Laser Scanners'. *Photogrammetric Record* 21: 141–160.

Lucieer, A., D. Turner, D.H. King, and Et Al. 2014. 'Using an Unmanned Aerial Vehicle (UAV) to Capture Micro-Topography of Antarctic Moss Beds'. *International Jour-nal of Applied Earth Observation and Geoinformation* 27 (Part A: 53–62.

Malet, J.-P., O. Maquaire, and E. Calais. 2002. 'The Use of Global Positioning System Techniques for the Continuous Monitoring of Landslides'. *Geomorphology* 43: 33–54.

Marchi, L. et al. 1992. *Quaderni Di Ricerca N, 13 'Il Bacino Attrezzato Del Rio Cordon'*. ed. Dipartimento Foreste.

Metternicht, Graciela, Lorenz Hurni, and Radu Gogu. 2005. 'Remote Sensing of Landslides: An Analysis of the Potential Contribution to Geo-Spatial Systems for Hazard Assessment in Mountainous Environments'. *Remote Sensing of Environment* 98(2–3): 284–303.

Monserrat, O., and M. Crosetto. 2008. 'Deformation Measurement Using Terrestrial Laser Scanning Data and Least Squares 3D Surface Matching'. *ISPRS Journal of Photogrammetry and Remote Sensing* 63 (1): 142–154.

Niethammer, U. et al. 2010. 'Uav - Based Remote Sensing of Landslides'. *International Archives of Photogrammetry, Remote Sensing and Spatial Information Sciences. Vol. XXXVIII, Part 5. Commission V Symposium* XXXVIII(2005): 496–501.

———. 2011. 'UAV-Based Re- Mote Sensing of the Super-Sauze Landslide: Evaluation and Results'. *Eng. Geol.* 128: 2–11.

Ouédraogo, M.M., A. Degré, C. Debouche, and J. Lisein. 2014. 'The Evaluation of Unmanned Aerial System-Based Photogrammetry and Terrestrial Laser Scanning to Generate DEMs of Agricultural Watersheds'. *Geomorphology* 214: 339–355.

Prosdocimi, Massimo et al. 2015. 'Bank Erosion in Agricultural Drainage Networks: New Challenges from Structure-from-Motion Photogrammetry for Post-Event Analysis'. *Earth Surface Processes and Landforms* 40(14): 1891–1906.

Rainato, R. et al. 2016. 'Three Decades of Monitoring in the Rio Cordon Instrumented Basin: Sediment Budget and Temporal Trend of Sediment Yield'. *Geomorphology*. http://www.sciencedirect.com/science/article/pii/S0169555X16301039.

Razak, Khamarrul Azahari et al. 2011. 'Airborne Laser Scanning of Forested Landslides Characterization: Terrain Model Quality and Visualization'. *Geomorphology* 126(1–2): 186–200. http://dx.doi.org/10.1016/j.geomorph.2010.11.003.

———. 2013. 'Generating an Optimal DTM from Airborne Laser Scanning Data for Landslide Mapping in a Tropical Forest Environment'. *Geomorphology* 190: 112–25. http://dx.doi.org/10.1016/j.geomorph.2013.02.021.

Schürch, P. et al. 2011. 'Detection of Surface Change in Complex Topography Using Terrestrial Laser Scanning: Application to the Illgraben Debris-Flow Channel'. *Earth Surf. Process. Landf.* 36: 1847–1859.

Shan, J, and K. Toth. 2008. 'Topographic Laser Ranging and Scanning: Principles and Processing'. *CRC Press, Taylor & Francis Group*.

Singhroy, V. 2009. 'Satellite Remote Sensing Applications for Landslde Detection and Monitoring'. In *Sassa K, Canuti P (Eds) Landslides—disaster Risk Reduction.*, Berlin/Heidelberg, 143–158.

Squarzoni, C., C. Delacourt, and P. Allemand. 2005. 'Differential Single-Frequency GPS Monitoring of the La Valette Landslide (French Alps)'. *Engineering Geology* 79: 215–229.

Stow, R. 1996. 'Application of SAR Interferometry to the Imaging and Measurement of Neotectonic Move- Ment Applied to Mining and Other Subsidence/downwarp Modeling'. In *Fringe 96 Proceedings ESA Workshop on Applications of ERS SAR Interferometry*, Zurich, Sw.

Stumpf, A., J.-P. Malet, P. Allemand, and P. Ullrich. 2014. 'Surface Reconstruction and Landslide Displacement Monitoring with Pléiades VHR Satellite Images'. *ISPRS J. Photogramm. Remote Sens.* 95: 1–12.

Tarchi, D. et al. 2003. 'Landslide Monitoring by Using Ground-Based SAR Interferometry: An Example of Application to the Tessina Landslide in Italy'. *Eng Geol* 68: 15–30.

Teza, G., A. Galgaro, N. Zaltron, and R. Genevois. 2007. 'Terrestrial Laser Scanner to Detect Landslide Displacement Fields: A New Approach'. *Int. J. Remote Sens.* 28: 3425–3446.

Travelletti, J et al. 2008. 'Monitoring Landslide Displacements during a Controlled Rain Experiment Using a Long-Range Terrestrial Laser Scanning (TLS)'. *The International Archives of the Photogrammetry, Remote Sensing and Spatial Information Sciences* 2007(July): 1–6. http://eost.u-strasbg.fr/omiv/Publications/Travelletti_2008_ISPRS.pdf.

Travelletti, J. et al. 2012. 'Correlation of Multi-Temporal Ground-Based Optical Images for Landslide Monitoring: Application, Potential and Limitations'. *ISPRS Journal of Photogrammetry and Remote Sensing* 70: 39–55. http://dx.doi.org/10.1016/j.isprsjprs.2012.03.007.

Turner, Darren, Arko Lucieer, and Steven M. de Jong. 2015. 'Time Series Analysis of Landslide Dynamics Using an Unmanned Aerial Vehicle (UAV)'. *Remote Sensing* 7(2): 1736–57.

Vallet, J., and J. Skaloud. 2004. 'Development and Experiences with a Fully-Digital Handheld Mapping System Operated from a Helicopter'. *Int Archi Photogramm Remote Sens* 35 (B5): 791–796.

Varnes, D J. 1978. 'Slope Movement Types and Processes'. *Transportation Research Board Special Report* (176): 11–33.

Verhoeven, G. 2011. 'Taking Computer Vision aloft—Archaeological Three-Dimensional Reconstructions from Aerial Photographs with Photo- Scan'. *Archaeol. Prospect.* 18: 67–73.

Wang, Guoquan et al. 2013. 'Delineating and Defining the Boundaries of an Active Landslide in the Rainforest of Puerto Rico Using a Combination of Airborne and Terrestrial LIDAR Data'. *Landslides* 10(4): 503–13.

Welty, E., W. T. Pfeffer, and Y. Ahn. 2010. 'Something for Everyone: Quantifying Evolving (Glacial) Landscapes with Your Camera, Abstract IN33B-1314'. In *2010 Fall Meeting, AGU,* San Francisco, California.

Westoby, M. J. et al. 2012. '"Structure-from-Motion" Photogrammetry: A Low-Cost, Effective Tool for Geoscience Applications'. *Geomorphology* 179: 300–314. http://dx.doi.org/10.1016/j.geomorph.2012.08.021.

Wheaton, Joseph M., James Brasington, Stephen E. Darby, and David A. Sear. 2010. 'Accounting for Uncertainty in DEMs from Repeat Topographic Surveys: Improved Sediment Budgets'. *Earth Surface Processes and Landforms* 35(2): 136–56.

Whitehead, K., B.J. Moorman, and C.H. Hugenholtz. 2013. 'Low-Cost, on-Demand Aerial Photo-Grammetry for Glaciological Measurement'. *Cryosphere Discuss.* 7: 3043–3057.

WMO, World Meteorological Organization, and United Nations Educational and Scientific Organization UNESCO. 1998. IHP/OHP-Berichte *International Glossary of Hydrology*. http://www.wmo.int/pages/prog/hwrp/publications/international_glossary/385_IGH_2012.pdf.

WEBSITES

http://www.direttivaacque.minambiente.it/

http://criticalzone.org

www.gislounge.com

https://www.researchgate.net

http://gcd.joewheaton.org/

www.agisoft.com

ANNEX

ANNEX 1 DoD 2011-2006

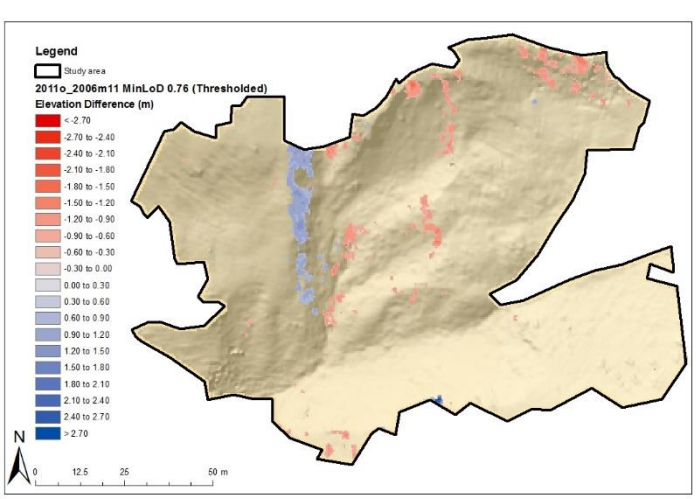

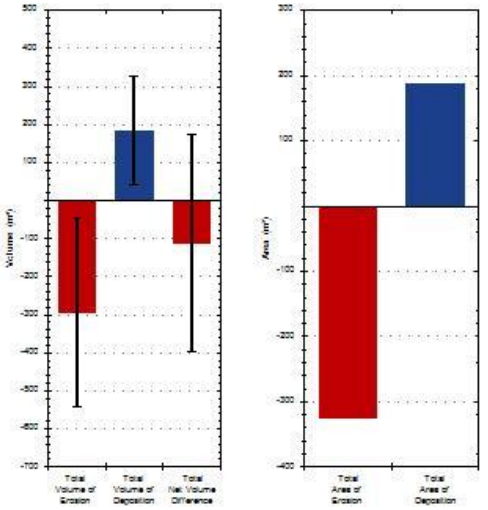

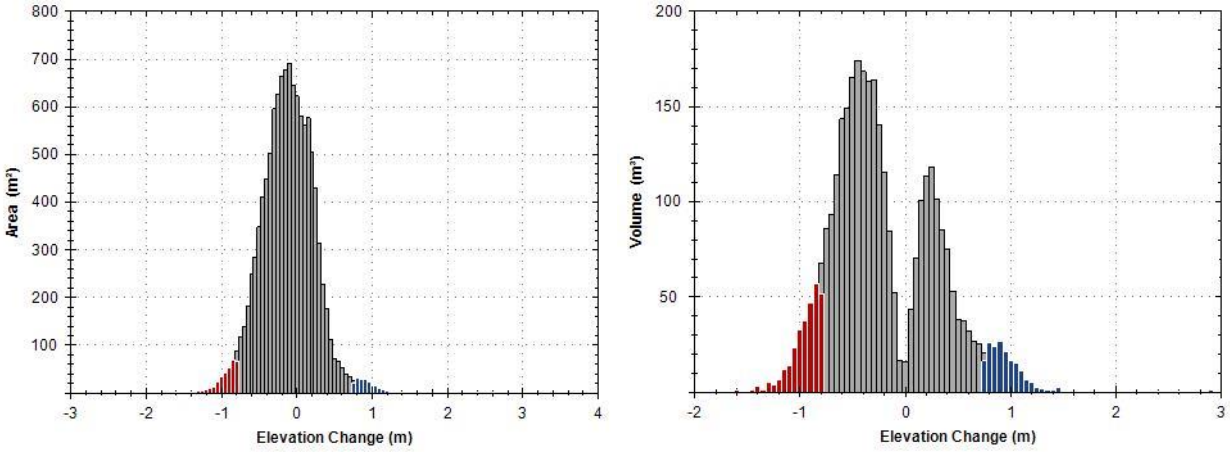

Attribute	Raw	Thresholded		± Error Vo	% Error
AREAL:					
Total Area of Erosion (m²)	6,932.25	326.25			
Total Area of Deposition (m²)	4,564.75	188.50			
Total Area of Detectable Change (m²)	NA	514.75			
Total Area of Interest (m²)	11,497.00	NA			
Percent of Area of Interest with Detectable Change	NA	4.48%			
VOLUMETRIC:					
Total Volume of Erosion (m³)	2,141.91	296.36	±	247.95	83.66
Total Volume of Deposition (m³)	1,122.78	182.71	±	143.26	78.41
Total Volume of Difference (m³)	3,264.69	479.08	±	391.21	81.66
Total Net Volume Difference (m³)	-1,019.12	-113.65	±	286.36	-251.97
VERTICAL AVERAGES:					
Average Depth of Erosion (m)	0.31	0.91	±	0.76	83.66
Average Depth of Deposition (m)	0.25	0.97	±	0.76	78.41
Average Total Thickness of Difference (m) for Area of Interest	0.28	0.04	±	0.03	81.66
Average Net Thickness of Difference (m) for Area of Interest	-0.09	-0.01	±	0.02	-251.97
Average Total Thickness of Difference (m) for Area with Detectable Change	NA	0.93	±	0.76	81.66
Average Net Thickness of Difference (m) for Area with Detectable Change	NA	-0.22	±	0.56	-251.97
PERCENTAGES (BY VOLUME):					
Percent Erosion	65.61	61.86			
Percent Deposition	34.39	38.14			
Percent Imbalance (departure from equilibium)	-15.61	-11.86			
Net to Total Volume Ratio	-31.22	-23.72			

ANNEX 2 DoD 2016-2011

A - DoD 0.5m

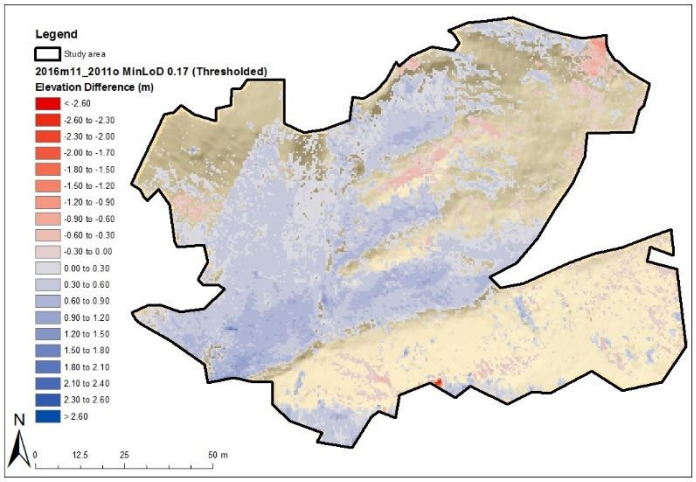

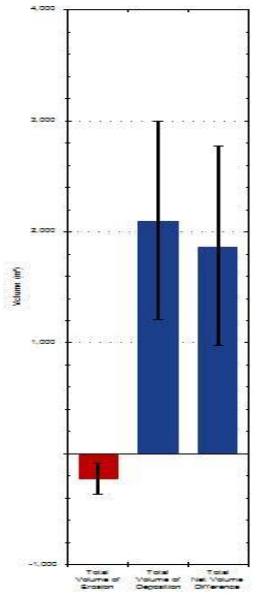

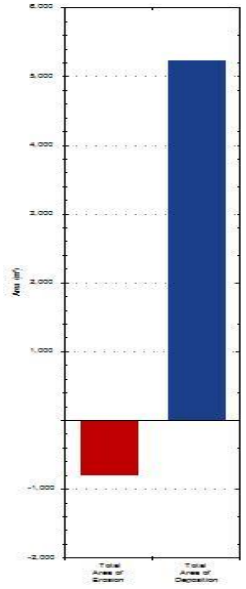

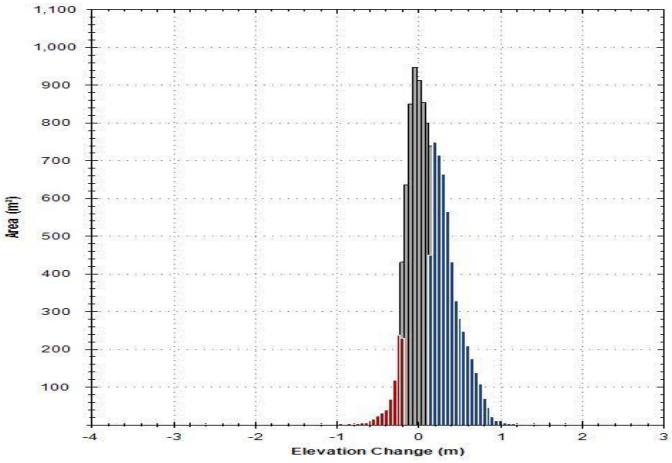

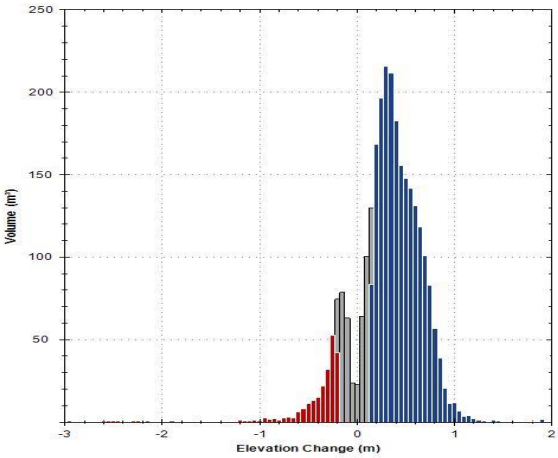

Attribute	Raw	Thresholded		± Error Vo	% Error
AREAL:					
Total Area of Erosion (m²)	3,435.50	800.00			
Total Area of Deposition (m²)	8,099.25	5,243.00			
Total Area of Detectable Change (m²)	NA	6,043.00			
Total Area of Interest (m²)	11,534.75	NA			
Percent of Area of Interest with Detectable Change	NA	52.39%			
VOLUMETRIC:					
Total Volume of Erosion (m³)	426.43	228.64	±	136.00	59.48
Total Volume of Deposition (m³)	2,331.80	2,098.59	±	891.31	42.47
Total Volume of Difference (m³)	2,758.23	2,327.23	±	1,027.31	44.14
Total Net Volume Difference (m³)	1,905.37	1,869.95	±	901.63	48.22
VERTICAL AVERAGES:					
Average Depth of Erosion (m)	0.12	0.29	±	0.17	59.48
Average Depth of Deposition (m)	0.29	0.40	±	0.17	42.47
Average Total Thickness of Difference (m) for Area of Interest	0.24	0.20	±	0.09	44.14
Average Net Thickness of Difference (m) for Area of Interest	0.17	0.16	±	0.08	48.22
Average Total Thickness of Difference (m) for Area with Detectable Change	NA	0.39	±	0.17	44.14
Average Net Thickness of Difference (m) for Area with Detectable Change	NA	0.31	±	0.15	48.22
PERCENTAGES (BY VOLUME):					
Percent Erosion	15.46	9.82			
Percent Deposition	84.54	90.18			
Percent Imbalance (departure from equilibium)	34.54	40.18			
Net to Total Volume Ratio	69.08	80.35			

B - DoD 0.2 m

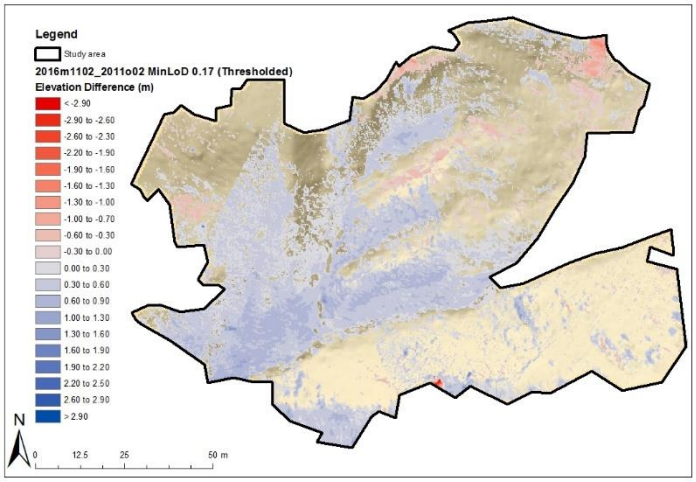

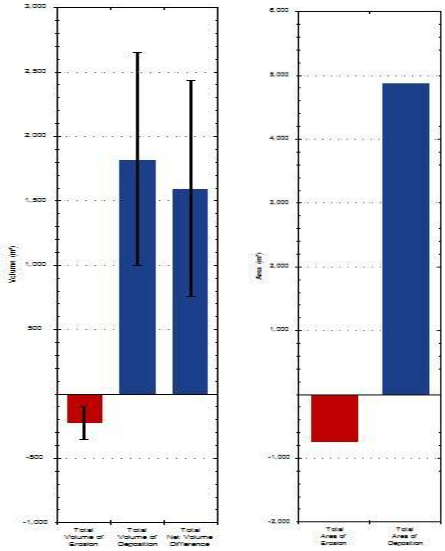

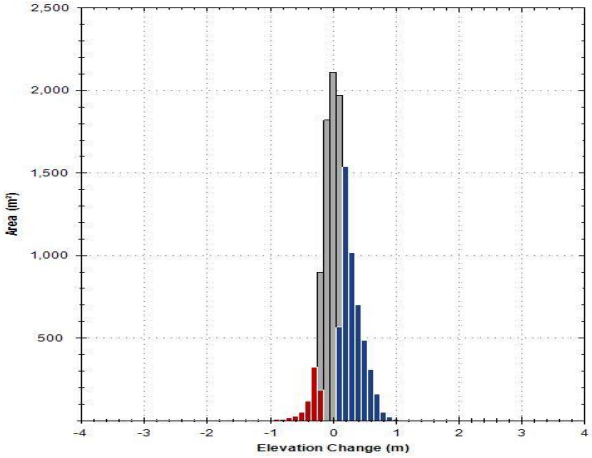

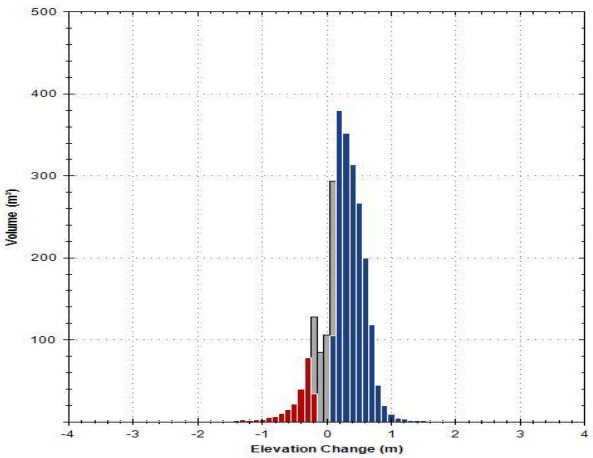

Attribute	Raw	Thresholded		± Error Vo	% Error
AREAL:					
Total Area of Erosion (m²)	3,280.44	745.60			
Total Area of Deposition (m²)	8,383.00	4,869.72			
Total Area of Detectable Change (m²)	NA	5,615.32			
Total Area of Interest (m²)	11,663.44	NA			
Percent of Area of Interest with Detectable Change	NA	48.14%			
VOLUMETRIC:					
Total Volume of Erosion (m³)	405.85	227.33	±	126.75	55.76
Total Volume of Deposition (m³)	2,115.92	1,821.13	±	827.85	45.46
Total Volume of Difference (m³)	2,521.78	2,048.47	±	954.60	46.60
Total Net Volume Difference (m³)	1,710.07	1,593.80	±	837.50	52.55
VERTICAL AVERAGES:					
Average Depth of Erosion (m)	0.12	0.30	±	0.17	55.76
Average Depth of Deposition (m)	0.25	0.37	±	0.17	45.46
Average Total Thickness of Difference (m) for Area of Interest	0.22	0.18	±	0.08	46.60
Average Net Thickness of Difference (m) for Area of Interest	0.15	0.14	±	0.07	52.55
Average Total Thickness of Difference (m) for Area with Detectable Change	NA	0.36	±	0.17	46.60
Average Net Thickness of Difference (m) for Area with Detectable Change	NA	0.28	±	0.15	52.55
PERCENTAGES (BY VOLUME):					
Percent Erosion	16.09	11.10			
Percent Deposition	83.91	88.90			
Percent Imbalance (departure from equilibium)	33.91	38.90			
Net to Total Volume Ratio	67.81	77.80			

ANNEX 3 DoD 2016-2006

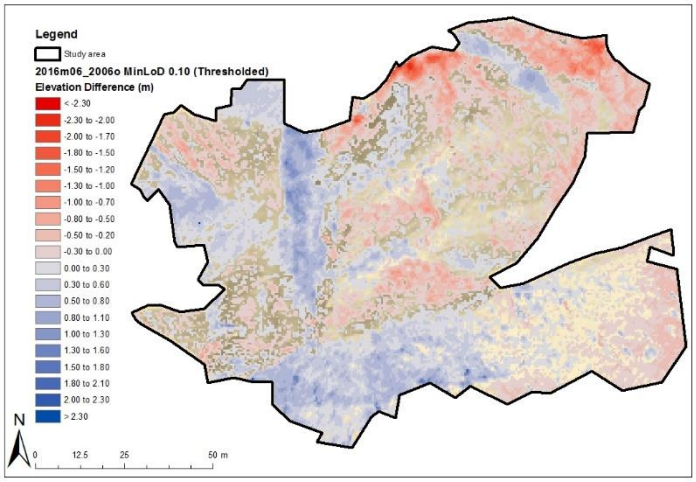

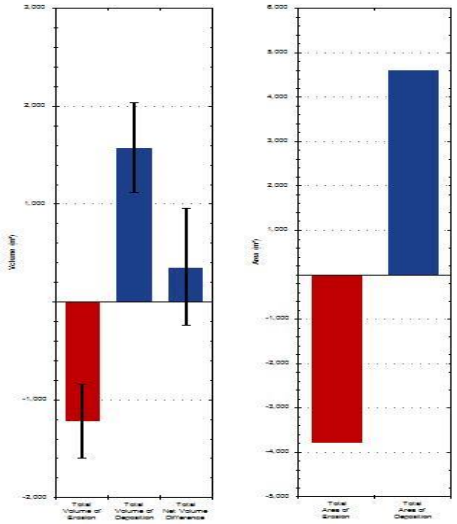

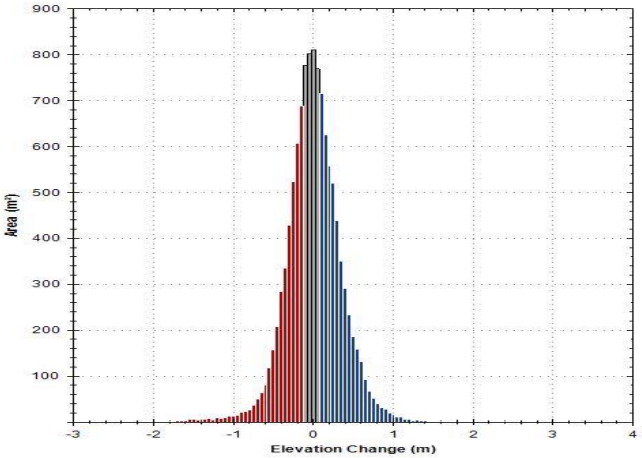

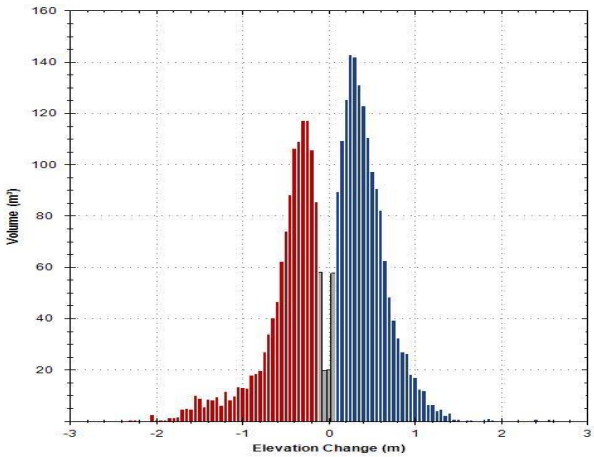

Attribute	Raw	Thresholded		± Error Vo	% Error
AREAL:					
Total Area of Erosion (m²)	5,354.50	3,776.00			
Total Area of Deposition (m²)	6,179.50	4,602.50			
Total Area of Detectable Change (m²)	NA	8,378.50			
Total Area of Interest (m²)	11,534.00	NA			
Percent of Area of Interest with Detectable Change	NA	72.64%			
VOLUMETRIC:					
Total Volume of Erosion (m³)	1,298.60	1,220.69	±	377.60	30.93
Total Volume of Deposition (m³)	1,650.81	1,572.88	±	460.25	29.26
Total Volume of Difference (m³)	2,949.41	2,793.57	±	837.85	29.99
Total Net Volume Difference (m³)	352.21	352.19	±	595.32	169.03
VERTICAL AVERAGES:					
Average Depth of Erosion (m)	0.24	0.32	±	0.10	30.93
Average Depth of Deposition (m)	0.27	0.34	±	0.10	29.26
Average Total Thickness of Difference (m) for Area of Interest	0.26	0.24	±	0.07	29.99
Average Net Thickness of Difference (m) for Area of Interest	0.03	0.03	±	0.05	169.03
Average Total Thickness of Difference (m) for Area with Detectable Change	NA	0.33	±	0.10	29.99
Average Net Thickness of Difference (m) for Area with Detectable Change	NA	0.04	±	0.07	169.03
PERCENTAGES (BY VOLUME):					
Percent Erosion	44.03	43.70			
Percent Deposition	55.97	56.30			
Percent Imbalance (departure from equilibium)	5.97	6.30			
Net to Total Volume Ratio	11.94	12.61			

ANNEX 4 DoD 2011-2010

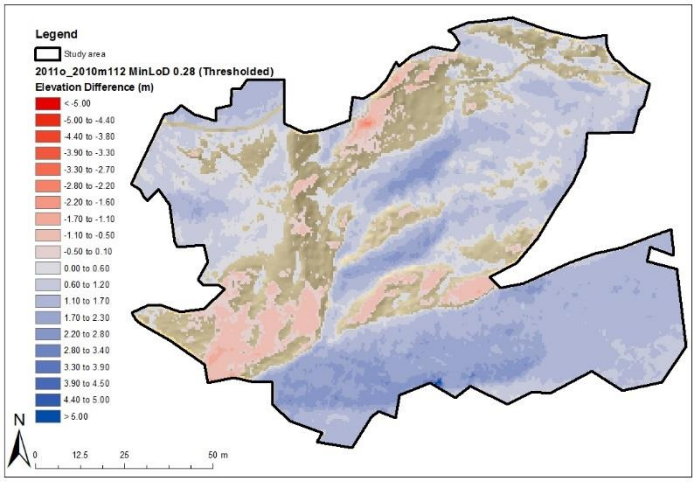

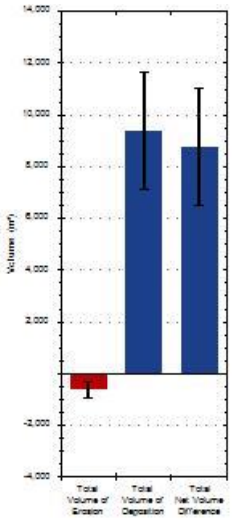

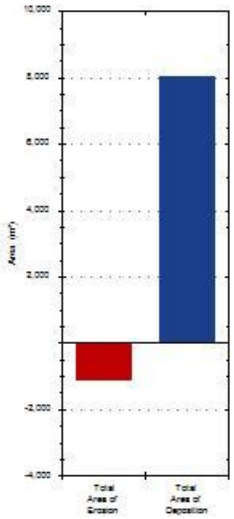

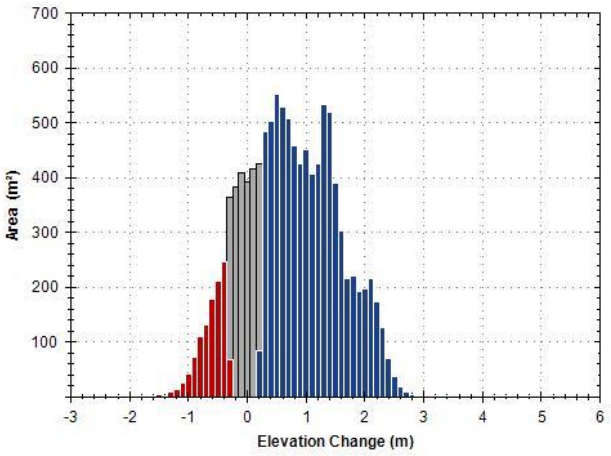

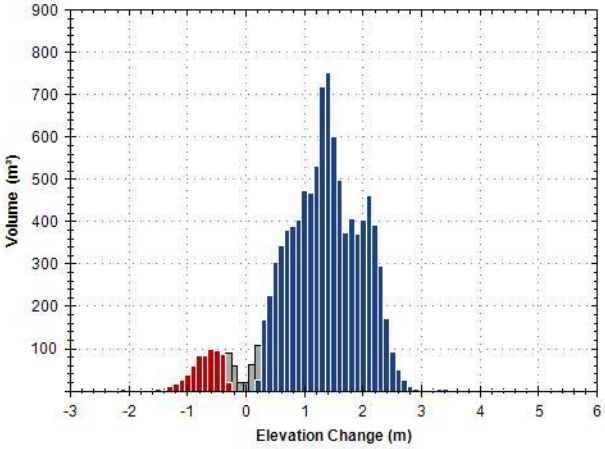

Attribute	Raw	Thresholded		± Error Vo	% Error
AREAL:					
Total Area of Erosion (m²)	2,202.50	1,111.25			
Total Area of Deposition (m²)	9,207.75	8,059.50			
Total Area of Detectable Change (m²)	NA	9,170.75			
Total Area of Interest (m²)	11,410.25	NA			
Percent of Area of Interest with Detectable Change	NA	80.37%			
VOLUMETRIC:					
Total Volume of Erosion (m³)	780.90	632.20	±	311.15	49.22
Total Volume of Deposition (m³)	9,545.26	9,381.12	±	2,256.66	24.06
Total Volume of Difference (m³)	10,326.17	10,013.32	±	2,567.81	25.64
Total Net Volume Difference (m³)	8,764.36	8,748.92	±	2,278.01	26.04
VERTICAL AVERAGES:					
Average Depth of Erosion (m)	0.35	0.57	±	0.28	49.22
Average Depth of Deposition (m)	1.04	1.16	±	0.28	24.06
Average Total Thickness of Difference (m) for Area of Interest	0.90	0.88	±	0.23	25.64
Average Net Thickness of Difference (m) for Area of Interest	0.77	0.77	±	0.20	26.04
Average Total Thickness of Difference (m) for Area with Detectable Change	NA	1.09	±	0.28	25.64
Average Net Thickness of Difference (m) for Area with Detectable Change	NA	0.95	±	0.25	26.04
PERCENTAGES (BY VOLUME):					
Percent Erosion	7.56	6.31			
Percent Deposition	92.44	93.69			
Percent Imbalance (departure from equilibium)	42.44	43.69			
Net to Total Volume Ratio	84.88	87.37			

ANNEX 5 DoD 2010-2006

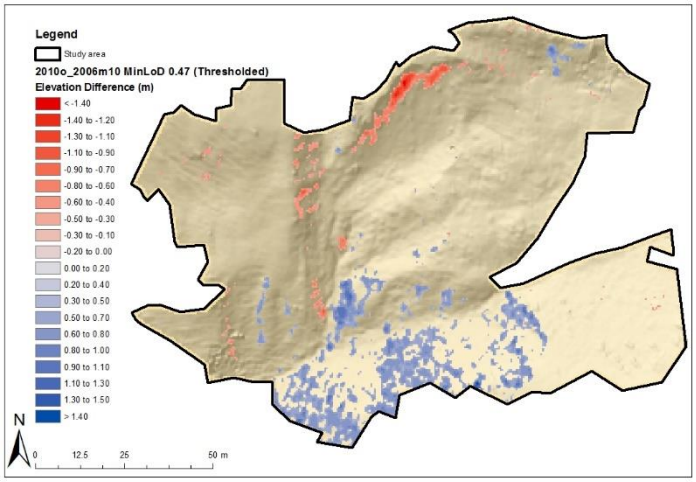

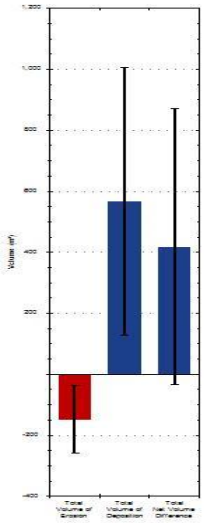

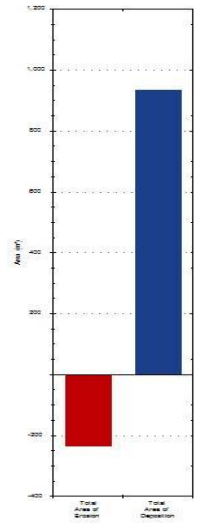

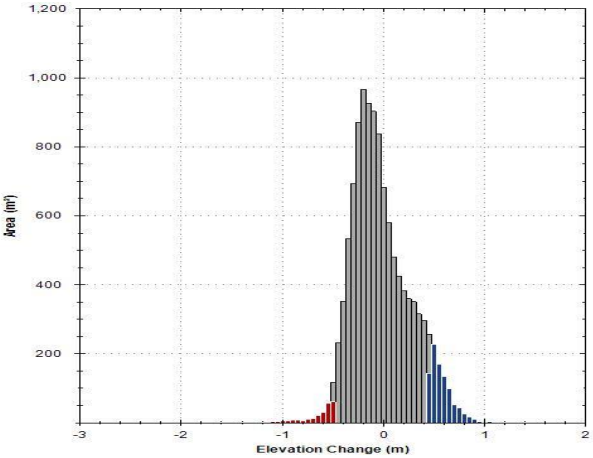

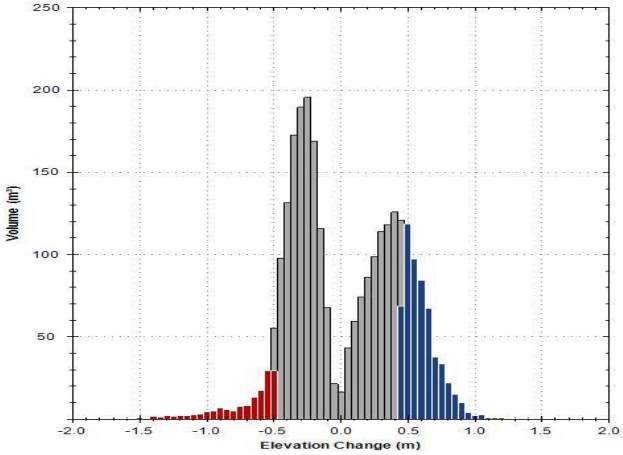

Attribute	Raw	Thresholded		± Error Vo	% Error
AREAL:					
Total Area of Erosion (m²)	6,605.25	236.50			
Total Area of Deposition (m²)	4,917.75	934.25			
Total Area of Detectable Change (m²)	NA	1,170.75			
Total Area of Interest (m²)	11,523.00	NA			
Percent of Area of Interest with Detectable Change	NA	10.16%			
VOLUMETRIC:					
Total Volume of Erosion (m³)	1,336.38	149.65	±	111.16	74.28
Total Volume of Deposition (m³)	1,354.71	566.60	±	439.10	77.50
Total Volume of Difference (m³)	2,691.09	716.24	±	550.25	76.82
Total Net Volume Difference (m³)	18.32	416.95	±	452.95	108.63
VERTICAL AVERAGES:					
Average Depth of Erosion (m)	0.20	0.63	±	0.47	74.28
Average Depth of Deposition (m)	0.28	0.61	±	0.47	77.50
Average Total Thickness of Difference (m) for Area of Interest	0.23	0.06	±	0.05	76.82
Average Net Thickness of Difference (m) for Area of Interest	0.00	0.04	±	0.04	108.63
Average Total Thickness of Difference (m) for Area with Detectable Change	NA	0.61	±	0.47	76.82
Average Net Thickness of Difference (m) for Area with Detectable Change	NA	0.36	±	0.39	108.63
PERCENTAGES (BY VOLUME):					
Percent Erosion	49.66	20.89			
Percent Deposition	50.34	79.11			
Percent Imbalance (departure from equilibium)	0.34	29.11			
Net to Total Volume Ratio	0.68	58.21			

ANNEX 6 DoD 2016-2010

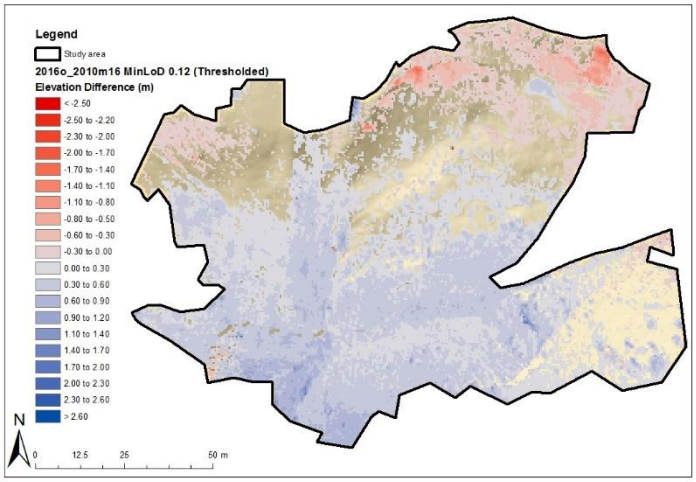

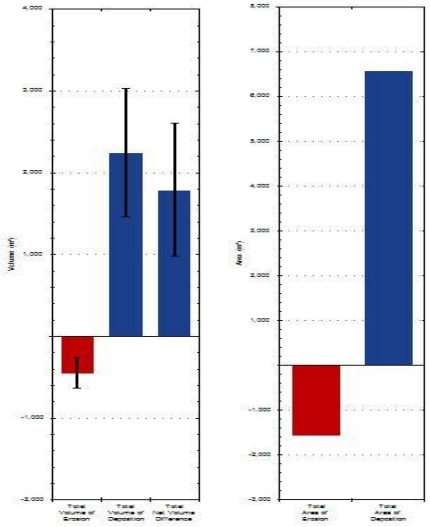

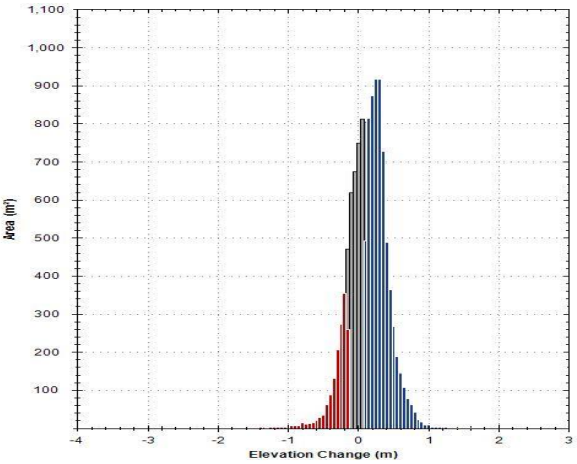

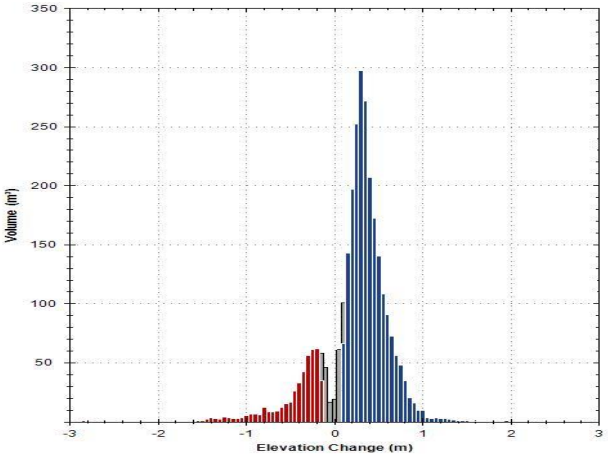

Attribute	Raw	Thresholded		± Error Vo	% Error
AREAL:					
Total Area of Erosion (m²)	3,072.75	1,566.00			
Total Area of Deposition (m²)	8,439.25	6,567.50			
Total Area of Detectable Change (m²)	NA	8,133.50			
Total Area of Interest (m²)	11,512.00	NA			
Percent of Area of Interest with Detectable Change	NA	70.65%			
VOLUMETRIC:					
Total Volume of Erosion (m³)	538.59	452.46	±	187.92	41.53
Total Volume of Deposition (m³)	2,353.97	2,239.33	±	788.10	35.19
Total Volume of Difference (m³)	2,892.56	2,691.78	±	976.02	36.26
Total Net Volume Difference (m³)	1,815.38	1,786.87	±	810.19	45.34
VERTICAL AVERAGES:					
Average Depth of Erosion (m)	0.18	0.29	±	0.12	41.53
Average Depth of Deposition (m)	0.28	0.34	±	0.12	35.19
Average Total Thickness of Difference (m) for Area of Interest	0.25	0.23	±	0.08	36.26
Average Net Thickness of Difference (m) for Area of Interest	0.16	0.16	±	0.07	45.34
Average Total Thickness of Difference (m) for Area with Detectable Change	NA	0.33	±	0.12	36.26
Average Net Thickness of Difference (m) for Area with Detectable Change	NA	0.22	±	0.10	45.34
PERCENTAGES (BY VOLUME):					
Percent Erosion	18.62	16.81			
Percent Deposition	81.38	83.19			
Percent Imbalance (departure from equilibium)	31.38	33.19			
Net to Total Volume Ratio	62.76	66.38			